

BUBBLE DEPARTURE PHENOMENA ON MODIFIED SURFACES FOR ENHANCED POOL BOILING

Mahmudul Hasan
Student ID.: 1015102012F



Department of Mechanical Engineering
BANGLADESH UNIVERSITY OF ENGINEERING AND TECHNOLOGY
Dhaka, Bangladesh
June, 2018

**Bubble Departure Phenomena On Modified Surfaces For Enhanced
Pool Boiling**

By

Mahmudul Hasan

Student ID.: 1015102012F

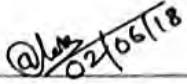
A Thesis Submitted in Partial Fulfillment of the Requirements for the Degree of
MASTER OF SCIENCE IN MECHANICAL ENGINEERING


Department of Mechanical Engineering
BANGLADESH UNIVERSITY OF ENGINEERING AND TECHNOLOGY
Dhaka, Bangladesh
June, 2018


CERTIFICATE OF THESIS APPROVAL

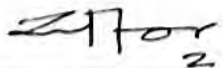
The thesis titled '**Bubble Departure Phenomena on Modified Surfaces for Enhanced Pool Boiling**' submitted by **Mahmudul Hasan, Roll No. 1015102012F**, Session: October 2015 has been accepted as satisfactory in partial fulfillment of the requirement for the Degree of **Master of Science in Mechanical Engineering** on 2 June, 2018.

BOARD OF EXAMINERS

1. 
_____ **Dr. Aloke Kumar Mozumder** **Chairman**
Professor (Supervisor)
Department of ME, BUET, Dhaka.

2. 
_____ **Dr. Md. Ashrafur Islam** **Member (Ex-officio)**
Professor and Head
Department of ME, BUET, Dhaka.

3. 
_____ **Dr. M. A. Rashid Sarkar** **Member**
Professor
Department of ME, BUET, Dhaka.

4. 
_____ **Brigadier General Md. Lutfur Rahman, Ph.D.** **Member (External)**
Vice Chancellor
Bangladesh Army University of Science and Technology (BAUST).
Saidpur Cantonment, Saidpur, Nilphamari.

CERTIFICATE OF RESEARCH

This is to certify that the work presented in this thesis is carried out by the author under the supervision of Dr. Alope Kumar Mozumder, Professor of the Department of Mechanical Engineering, Bangladesh University of Engineering and Technology, Dhaka, Bangladesh.

Mahmudul Hasan

Dr. Alope Kumar Mozumder

Mahmudul Hasan

DECLARATION

It is hereby declared that this thesis/project or any part of it has not been submitted elsewhere for the award of any degree or diploma.

02/06/2018

Date

Mahmudul Hasan

Mahmudul Hasan

Author

ACKNOWLEDGMENT

I am very grateful and indebted to my supervisor Dr. Alope Kumar Mozumder, Professor of the Department of Mechanical Engineering, Bangladesh University of Engineering and Technology, for his kind supervision, constant guidance, encouragement, support and thoughtful discussion throughout the entire research work.

I am also grateful to the Department of Mechanical Engineering, BUET for providing necessary lab facilities for the research.

I would also like to thank my parents for their help and mental support during my research.

Author

ABSTRACT

This research work explores bubble departure phenomena on different modified surfaces for enhanced pool boiling of water. Experiments were conducted for understanding bubble interaction with surfaces of different topography. The experiments were conducted in a controlled environment. Important parameters of pool boiling i.e. bubble departure diameter and bubble departure frequency were measured and analyzed to understand the mechanism of pool boiling and associated heat transfer. High speed video camera was employed to capture bubble phenomena on boiling surface. Three different surfaces have been used for experimentation as plain surface, pitted surface and finned surface. Copper is used as boiling surface and fin material. The setup was designed in such a way that the effect of surface topography can be precisely measured.

It has been observed that bubble departure phenomena not only depends on the supplied heat flux, but also on the surface topography, bubble merging and nucleation site density. Here it is revealed that with higher heat flux bubble departure diameter and bubble departure frequency generally increases along with heat transfer coefficient. But the increment is not linear as it seems. Although with the increase of heat flux, bubble departure diameter increases, there are other factors like surface tension, acting forces due to fluid motion, drag force and surface topography that affects the phenomena. These factors also affects the heat transfer coefficient of the system.

From the visual observation of the images of high speed video camera and analysis of obtained data, an empirical correlation has been proposed that can well predict the bubble departure diameter in pool boiling for different modified surfaces.

NOMENCLATURE

A = Area (m^2)
Ar = Archimedes number
Bo = Bond Number
 c_p = Specific heat at constant pressure ($\text{J.kg}^{-1}.\text{K}^{-1}$)
d, d_b = Bubble diameter (m)
f, f_d = Bubble departure frequency (Hz)
g = Gravity (m.s^{-2})
h = Heat transfer coefficient ($\text{W.m}^{-2}.\text{K}$)
 h_{fg} = Latent heat of vaporization (J.kg^{-1})
I = Electric Current, Ampere (A)
Ja = Jacob Number
k = Thermal conductivity ($\text{W.m}^{-1}.\text{K}^{-1}$)
P = Pressure (Pa)
Pr = Prandtl number
q = Heat flux (W/m^2)
T = Temperature (K)
t = Time (s)
 T_{sat} = Saturation Temperature ($^{\circ}\text{C}$)
 T_w = Surface Temperature ($^{\circ}\text{C}$)
V = Voltage, Volt (V)
 α = Thermal Diffusivity (m^2/s)
 ΔT = Wall Superheat (K)
 θ = Contact angle, degree
 μ = Dynamic Viscosity (kg/ms)
 ν = Viscous Diffusivity (m^2/s)
 ρ = Density (kg.m^{-3})
 σ = Surface tension (N.m^{-1})

Subscripts

l = liquid
v = vapor

Table of Contents

CERTIFICATE OF RESEARCH.....	iv
DECLARATION.....	v
ACKNOWLEDGMENT.....	vi
ABSTRACT.....	vii
NOMENCLATURE.....	viii
Chapter 1. INTRODUCTION.....	12
Chapter 2. LITERATURE REVIEW.....	15
Chapter 3. EXPERIMENTAL SETUP & METHODOLOGY.....	20
3.1 Construction.....	21
3.2 Camera.....	21
3.3 Boiling Surface.....	21
3.4 Methodology.....	22
3.5 Measurement Techniques.....	23
3.5.1 Bubble Departure Diameter.....	24
3.5.2 Bubble Departure Frequency.....	27
3.5.3 Wall-Temperature.....	27
3.5.4 Heat Flux.....	27
Chapter 4. RESULT & DISCUSSION.....	28
4.1 Bubble Departure Diameter.....	28
4.2 Bubble Departure Frequency.....	33
4.3 Heat Transfer.....	38
Chapter 5. DEVELOPMENT OF CORRELATION.....	41
Chapter 6. CONCLUSION & RECOMMENDATION.....	45
6.1 Conclusion.....	45
6.2 Recommendation.....	46
REFERENCE.....	47
APPENDIX - I: SPECIFICATION OF EQUIPMENT.....	49
APPENDIX - II: DATA TABLES.....	51
APPENDIX - III: SAMPLE CALCULATION.....	55
APPENDIX - IV: IMAGES.....	57
APPENDIX - V: UNCERTAINTY ANALYSIS.....	63

List of Figures

Fig. 3.1: Experimental setup for pool boiling.....	20
Fig. 3.2: Various types of surfaces used for experiment.....	22
Fig. 3.3: Bubble deformation during detachment from surface [t=33 millisecond, ms].....	24
Fig. 3.4: Bubble merging before departure.....	25
Fig. 3.5: Bubble merging while neighboring bubble is detached [t=35ms].....	25
Fig. 3.6: Irregular shaped bubbles and merging at the ascend.....	26
Fig. 3.7: Formation of irregular shaped bubbles at the surface.....	26
Fig. 4.1: Variation of bubble departure diameter with the increase of heat flux on plain surface.....	28
Fig. 4.2: Birth, growth due to prolonged heat absorption and detachment of a bubble.....	29
Fig. 4.3: Variation of bubble departure diameter with respect to heat flux, compared with Hamzekhani's [6] predictive correlation.....	32
Fig. 4.4: Comparison of different surfaces' bubble diameter with respect to wall superheat.....	33
Fig. 4.5: Bubble departure frequency at different heat flux.....	34
Fig. 4.6: Wall superheat vs. heat flux plot for plain surfaces.....	35
Fig. 4.7: Wall superheat vs. heat flux plot for pitted surfaces.....	36
Fig. 4.8: Wall superheat vs. heat flux plot for finned surfaces.....	36
Fig. 4.9: Image obtained at 70 kW/m ² on pitted surface showing the formation of buoyant column	37
Fig. 4.10: Mushroom type vapor bubble formed by bubble merging.....	37
Fig. 4.11: Merging of bubbles in same site.....	38
Fig. 4.12: Heat transfer coefficient at different wall superheat for different surfaces.....	39
Fig. 4.13: Heat transfer coefficient at different heat flux level for different surfaces.....	39
Fig. 4.14: Merging of 3 bubble embryos into one in plain surface.....	40
Fig. 5.1: Bubble diameter from proposed equation vs. experimental bubble diameter for plain surface.....	43
Fig. 5.2: Bubble diameter from proposed equation vs. experimental bubble diameter for Pitted surface.....	43
Fig. 5.3: Bubble diameter from proposed equation vs. experimental bubble diameter for Finned surface.....	44

Index of Tables

Table 4.1: Visuals of bubbles on different surface at different heat flux level.....	32
Table 5.1: Error rate of proposed empirical correlation with respect to experimentally obtained results:.....	43

Chapter 1.

INTRODUCTION

Bubble dynamics in pool boiling has been greatly studied since the first equation was derived by Lord Rayleigh [1]. Since then, a lot of improvements have been improvised. Yet, heat transfer enhancement in pool boiling is still not fully understood. In practice heat is transferred through a solid surface to make the vaporization of liquid possible. As more heat is added, the liquid adjacent to the surface exceeds the equilibrium saturation temperature. Since the temperature at the surface is at the highest, vapor embryo starts to occur at the interface of the solid-liquid. Formation of vapor embryo at the solid-liquid interface is one type of heterogeneous nucleation. Vapor embryos continue to grow and create bubble. It is true that various enhanced surface is being used, but the basic understanding of the phenomena is still at its beginning stage. This is partly because of the diverse surface types and increasing variables that make it more complex. There have been a lot of studies that tried to explain the phenomena and establish a correlation. Most of the correlations are either simple with limited range of application or so complex that it requires iterative procedure [2]. Fritz [3] model is considered one of the most reliable model. Ruckenstein [4] measured the bubble departure diameter as a function of wall-superheat. He also proposed a correlation based on his finding. By considering bubble growth mechanism Van Stralen and Zijl [5] also proposed an empirical correlation. The motivation behind the studies have been the formulation of a predictive models for bubble dynamics and heat transfer coefficient. It is widely known that different types of surfaces have different effects on pool boiling and heat transfer rate. Enhanced surfaces can greatly improve heat transfer rate. In this study pool boiling has been studied on different enhanced surfaces. Heterogeneous nucleation is the main focus for this study. Heterogeneous nucleation refers to the process of bubble formation in pits, scratches, grooves, fins on a heated surface submerged in a pool of liquid [6]. It is known that trapped gas in small cavities causes heterogeneous nucleation. The vapor bubble begins to form on the heated surface and starts to grow until it reaches a certain diameter and rise through the liquid. Also, higher heat transfer coefficient in nucleate pool boiling largely depends on heat transfer mechanism which is directly linked to bubble activity on the surface [7]. That's why almost all the correlation developed for modeling heat transfer phenomena contains a term related to bubble dynamics, especially bubble departure diameter. Beside bubble

departure diameter, literature showed that bubble departure frequency plays an important role in heat transfer phenomena [8]. It should also be noted that theoretical models for prediction of the nucleate boiling heat transfer coefficient are still at the early stage of development [9].

Predicting models are extremely helpful for various applications like cooling of nuclear reactor, refrigeration cycle, electronic component etc. Electronic devices are specially prone to heat damage. Thus, proper thermal management is extremely important in electronics components. The more and more compact devices are getting, the harder it's getting to manage heat situation. In 1974 the semiconductor standard was about 6 μm . In 2018 that standard has come to 7 nm and expected to be 5 nm in 2021. But as the components are getting smaller, the thermal heat dissipation is becoming complicated due to less surface to interact with. Now-a-days a home computer can easily have a microprocessor with 100W TDP (Thermal Design Power). This rapid development in the electronics industry requires high and efficient heat transfer in a small volume and space due to the closely packed microchips with higher thermal design power. Without proper heat dissipation system, the terminal solder component can get easily damaged or desoldered, rendering devices malfunctioned. It's inevitable that keeping these high performance devices cool with just heat sink and air flow is difficult. Another application of pool boiling heat transfer is in nuclear reactors. Since 1948 a lot of research and development has been carried out for nuclear power generation, specially for ships and submarines. As the vehicles uses water as their propulsion medium, it was very important to develop a design that involves water heat transfer technology. Later, with the increased use of nuclear power pant directed research towards the development of more efficient heat transfer system. Most cooling systems used in nuclear reactors uses water as a coolant to remove heat.

In this present study, three different surfaces have been used and studied. Previous studies focused on single surface lacks the scope to determine which single parameter affects the heat transfer mechanism most. Without comparison it's also hard to determine how bubbles plays the most significant role and how exactly surface modification causes the bubbles to act so differently. In this thesis, a setup was designed in such a way that the only variation is caused by surface geometry. A fixed size glass housing incorporated the boiling mechanism. The mechanism to supply heat to test pieces was designed to ensure minimum variation between surfaces keeping quantitative values intact. A high speed video camera was used to capture bubbles in slow motion to analyze later. For determining bubble departure diameter from high speed video, video were down-framed to 20~30

FPS so that individual bubbles can be accounted for. Two different methods were used to measure the diameters. One being pixel count per bubble along the diameter, considering bubble as sphere. On the other hand to make sure higher precision of the measurement, a reference scale was used in view of every video frame and bubble diameters were compared with it. To fully understand the phenomena of bubble dynamics in pool boiling, bubble departure frequencies were also measured from the high speed video. It's very tricky to determine bubble departure frequencies from video frames. At higher heat flux the bubbles becomes unstable due to fluid motion and the frequent merging at the surface as well as after leaving the surface while ascending to the top, makes it hard to accurately measure the frequency. With the help of the experimental data an empirical correlation has been proposed. All the acquired data have been analyzed for better understanding of the bubble departure phenomena.

The present study is mainly an experimental investigation; the primary aim of this study is to obtain a complete characteristics of bubble dynamics in pool boiling. Specific objectives of this study are as follows:

- i. To improve the visual understanding of bubble dynamics (bubble departure diameter, , bubble departure frequency, bubble area density) in pool boiling.
- ii. The experiment will be conducted with distilled water on three different geometry of hot copper surface for up to nucleate boiling temperature of water.
- iii. To inquire relations between various parameters of boiling and bubble dynamics, i.e. heat flux, heat transfer coefficient, bubble departure diameter, bubble departure frequency, bubble area density etc.
- iv. To compare the experimental results with previously predicted models
- v. To propose an empirical model based on experimental findings

The results of this analysis will improve the understanding for the heat transfer mechanism during boiling on high temperature solid. The knowledge of this bubble departure characteristics is necessary for the heat transfer equipment designer to avoid the possibility of burnout during boiling and to maximize the energy efficiency.

Chapter 2.

LITERATURE REVIEW

The initial idea of expressing the pool boiling phenomena mathematically in a predictive modeling came from Lord Rayleigh [1]. His first derivation was based on the initially controlled growth or collapse of vapor bubbles. The study was partially motivated by the sound of a tea kettle. Since then, it came to knowledge that the better understanding of bubble activities in pool boiling can deliver a highly accurate predictive model for pool boiling and accompanied heat transfer. In a study, Nukiyama [10] proposed that the amount of heat transmitted from heated surface to boiling water increases with the increase of wall superheat. But later researches showed that there are other variables like surface roughness and fluid type that play important roles in pool boiling. The following correlation by Fritz [3] is one of the widely used correlations.

$$d_b = 0.0208 \theta \sqrt{\frac{\sigma}{g(\rho_l - \rho_v)}} \quad (1)$$

The correlation is valid for both pure liquids and mixtures. But it's not particularly suitable for different surface geometry. Although θ is corrected for water to be 45° and for mixtures to be 35° , but no fitting parameter is included in the equation for different surface geometry. The following equation was proposed by Stephan and Abdelsalam [11] which is a modification of Fritz [3] model involving three dimensionless numbers namely Jacob (Ja), Prandtl (Pr), and Archimedes (Ar).

$$d_b = 0.25 \left[1 + \left(\frac{Ja}{Pr} \right)^2 \frac{100000}{Ar} \right]^{0.5} \sqrt{\frac{2\sigma}{g(\rho_l - \rho_v)}} \quad (2)$$

Here, Archimedes number is used to determine the motion of fluids due to density differences. It is a dimensionless number defined as the ratio of external forces to internal viscous forces and it can be expressed in the following form:

$$Ar = \frac{gL^3 \rho_l (\rho - \rho_l)}{\mu^2}$$

The Prandtl number (Pr) is another dimensionless number, defined as the ratio of momentum diffusivity to thermal diffusivity.

$$Pr = \frac{\nu}{\alpha}$$

Jakob number represents the ratio of sensible heat to latent heat absorbed (or released) during the phase change process. The Jakob number is represented as follows:

$$Ja = \frac{c_p \Delta T}{h_{fg}}$$

This model improved the prediction of bubble departure diameter over the Fritz [3] model. Cole and Rohsenow [12] also proposed similar model which gave the best result in the whole range of available experimental data for variety of liquid. Rohsenow [13] proposed that the heat transfer enhancement in boiling is the product of local liquid circulation near the heating surface promoted by successive bubble detachment and proposed the following correlation:

$$\frac{c_l \Delta T}{h_{fg}} = C_{sf} \left(\frac{g}{\mu_l h_{fg}} \sqrt{\frac{g \sigma}{g(\rho_l - \rho_v)}} \right)^{0.33} \left(\frac{c_l \mu_l}{k_l} \right)^{1.7} \quad (3)$$

Where, C_{sf} is the coefficient of equation.

Later Mikic and Rohsenow [14] proposed another correlation, this time including heating surface characteristics. This new correlation assumed that the main mechanism of heat transfer in pool boiling is transient heat conduction to and subsequent replacement of, the superheated layer around sites associated with bubble departure [14]. The correlation incorporated effects of heat transfer surface characteristics and allowed for different forms (q/A) versus wall superheat (ΔT) relations. Since properties of boiling surfaces in the reported experiments were not known, the required information about the boiling surface was found from q/A versus wall superheat (ΔT) data, at one pressure and then, using the same characteristics for the boiling surface, the correlation was applied to data for different pressures [14].

In an experimental investigation on heat transfer characteristic for an evaporator Mozumder and Kamal [15] experimented with three different evaporator surfaces i.e. Pin Finned Surface, Rectangular Finned Surface and Plain Surface with three different working fluids namely Acetone, Ethanol and Methanol. They concluded that surface geometry has immense effect on the heat transfer rate along with choice of working fluid.

In a study conducted by Leppert [16] it was pointed out that, as in the boiling heat transfer from a surface takes place mainly by a convective process to the liquid, high transfer rates can be achieved

with very small temperature differences due to high turbulence level which is produced in the liquid by vapor bubbles growing and leaving surface. He also noted that, in single phase heat transfer the process can be easily described by the viscosity, density, thermal conductivity and specific heat of the fluid, but it is very complicated to describe pool boiling and additional properties are required to consider.

Yeh and Griffith [17] showed that the area from which superheated layer is pumped away by a bubble is πd_b^2 , where d_b is bubble departure diameter. This hypothesis acted as a base for the Mikic and Rosenow [14] study.

Frederkin and Daniels [18] developed theoretical expression for the bubble departure diameter and bubble frequency during film boiling as:

$$d = \left[\frac{\sigma}{g(\rho_l - \rho_v)} \right]^{\frac{1}{2}} \quad (4)$$

This correlation is only applicable when a simple bubble pattern is produced [18]. On the basis of the kinematic studies, Frederkin and Daniels [18] concluded that vapor will be removed by gravity forces in the nucleate and film boiling regime, regardless of the heat flux magnitude and simple heat transport estimates can be made, in particular at the heat flux minimum, when $fd^{1/2}$ is approximately constant. Here bubble departure frequency is denoted by f and bubble departure diameter is denoted by d .

Fazel and Shafee [19] carried out an experimental study on pool boiling of electrolyte solutions. In Their study they showed that bubble diameter increases either by increasing heat flux at any constant concentration or by increasing concentration at any constant heat flux. Their correlation was specifically designed for electrolytic solutions. Fazel and Shafee [19] also hypothesized that the dynamic interfacial tension between the vapor and solution due to the swift evaporation of water during bubble generation to be less than the static equilibrium surface tension. Therefore, increasing the electrolyte concentration could increase the bubble departure diameter and decrease the active nucleatesite density.

Hamzekhiani et. al. [6] experimented with different working fluids namely water, methanol and ethanol at atmospheric pressure. They concluded that heat transfer coefficient of water is greater than both methanol and ethanol. They also concluded that heat transfer coefficient increases with the increase of heat flux for all the tested fluid. In their study they found that bubble departure diameter was larger than methanol and ethanol's bubble diameter. They also found that bubble departure diameter increases with the increase of heat flux in all liquid.

McHale and Garimella [8] experimentally investigated important bubble nucleation parameters during pool boiling on plain and rough surfaces. The characterized pool boiling by high bubble densities and numerous interactions between bubbles. Unlike previous studies they investigated characteristics of bubble nucleation from two different surfaces at various heat fluxes and compared them qualitatively. They measured the parameters from high speed videos. They also concluded that bubble diameter at departure was shown to increase with increasing wall superheat, but the surface roughness was also shown to have an influence along with bubble departure frequency. They found out that in general bubble departure frequency increased with heat flux. But the phenomena was not well predicted by any of the correlations considered from the literature. Along with bubble diameter and frequencies, nucleation site also tends to increase with the heat flux. However in their study they could well predict active site densities for both plain surface and roughened surface. They suggested that new bubble nucleation correlations should be developed which incorporate the important effect of surface roughness so that recent development in mechanistic modeling can be applied for a range of boiling surfaces [8].

In a study by Luke [20] involving experiment about interaction between bubble formation and heating, it was proposed that the densities of active nucleation sites calculated from the heat transfer measurements using model assumptions for the heat transfer near growing, detaching and sliding bubbles on horizontal evaporator tubes react sensitively on the input data of the departure diameter d_d and the frequency f of the bubbles. He also added that, considering the additional effects of the convective contributions to the heat transfer of the sliding bubbles and to the interactions of neighboring bubbles result in good agreement of calculated and measured site densities for smaller tubes. In certain ranges discrepancies still existed, especially for larger tubes and higher pressures. Their comparison of the cumulative size distribution of the active and potential nucleation sites demonstrates the same slope of the curve and that the critical radius of stable bubble nuclei is smaller than the average cavity size.

In another study conducted by Chu et. al. [21] described typical bubble behaviors from nucleation to lift-off. They observed that representative bubble corresponded to the bubble having the closest lift off diameter to the average lift-off diameter at each specific nucleation site under the given experimental conditions. As long as the bubbles were isolated, their behaviors in the vertical sub-cooled boiling flow were almost identical regardless of the differences in flow and heat flux conditions. The authors also observed that the bubble started to slide along the flow direction while attached to the heated surface. During this sliding process, the bubble grew continuously through heat transfers from both the heated surface and superheated liquid layer around the bubble periphery. After sliding a certain distance, the bubble was detached from the wall and moved into the subcooled bulk water flow, which is the instant of bubble lift-off. The author mentioned that from the very early period of bubble growth, the center of the bubble moved away from the nucleation site in a continuous manner.

Chapter 3.

EXPERIMENTAL SETUP & METHODOLOGY

For any experimental study, proper experimental setup is extremely important. In this experiment, the setup was designed in such a way that the boiling surface can be easily swapped out and replaced with different one with different topography so that the effect of surface topography is precisely reflected in the result. For better viewing and video recording at high speed the boiling vessel was chosen to be made of glass. It is difficult to acquire airtight setup when glass and metal are used together. The setup was properly sealed with enough silicon adhesive and rubber gasket. The whole setup was insulated for minimum heat loss. Figure 3.1 schematically demonstrates the experimental setup used in this study.

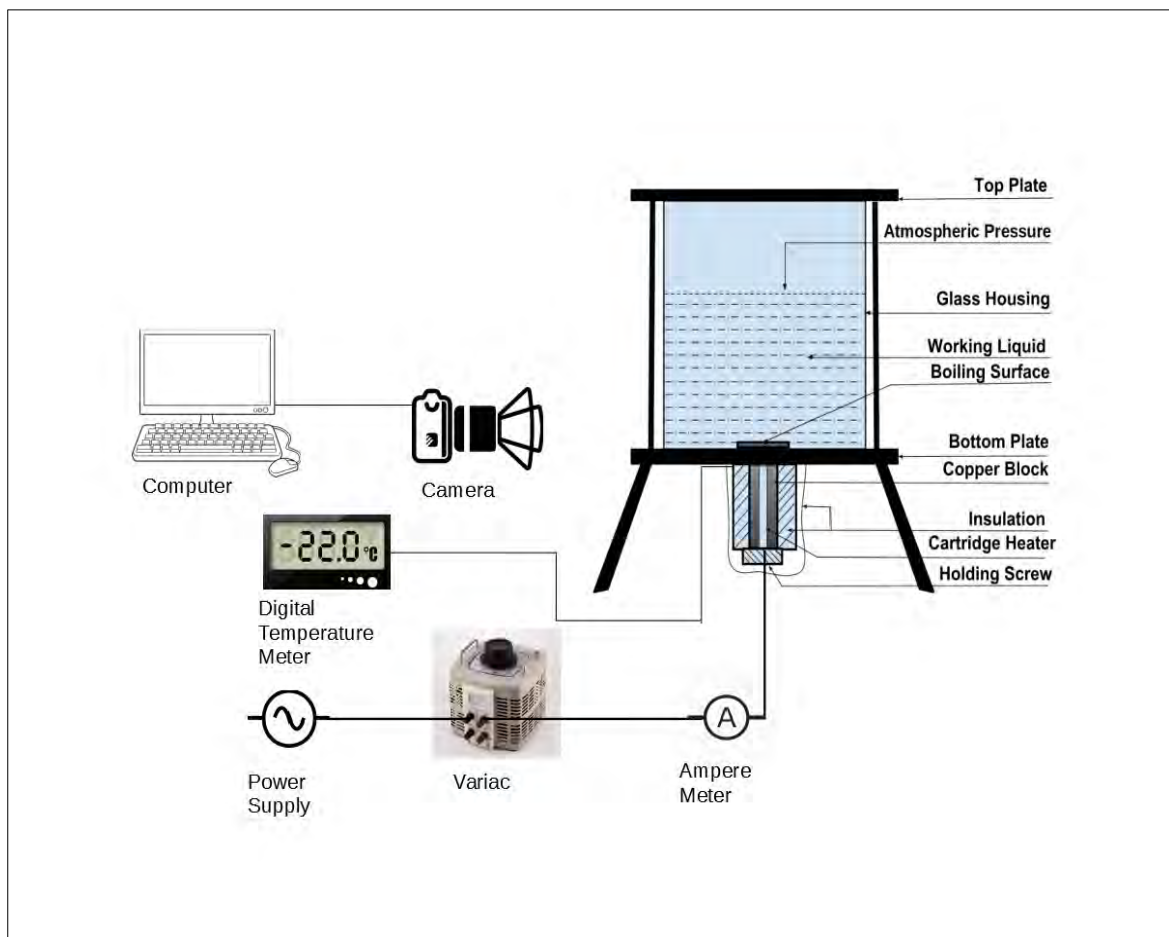


Fig. 3.1: Experimental setup for pool boiling

3.1 Construction

A temperature-resistance glass container was used to contain the working liquids; the bottom surface of the container was replaced by the working surface (which is actually a copper block with various surface geometry). Glass container is 113 mm in length and 97 mm in diameter. A curtiis heater was inserted inside the copper block through a fabricated hole, which acted as a source of heat. A variac was used to control the voltage of the heater thus controlling the power supply. The thermocouple was used to measure the temperature at different places.

3.2 Camera

A high-speed video camera (Phantom Miro EX4-4096MC, CMOS sensor, 8/12 bit color, 500-1260fps at full resolution (800x600 pixel), maximum 111,100fps at lowest resolution (32x16 pixel), ISO 4800(monochrome) and 1200(color)) was used to capture the boiling images.

3.3 Boiling Surface

Copper blocks were used as boiling surface. The blocks were 88 mm in height and 49 mm in diameter. The surface of the block which was treated as a plain surface when it is polished by zero grade emery paper and treated as a pitted surface when it is pitted 1 mm in depth and 2 pits/cm² with custom-designed tool to ensure desired experimental conditions. For the finned surface, the fins was inserted on the copper block by press-fit. The fins were made of copper, approximately 5 mm in height and 2.5 mm in diameter and approximately 3 fins/cm² in density. Figure 2 shows the images of different surface used in the setup. During the experiment, the liquid level was such that the fins were always at submerged condition which is the mandatory criteria for pool boiling. When the heater was on, the pressure above the working fluid was at atmospheric. After achieving the desired experimental conditions, the temperature, video images and the power consumption was recorded for analysis.

Although it is said that the plain surface is smooth and was worked on with zero grade emery paper to make sure maximum polishness, it is possible that it contained microscopic level pits, grains, scratch etc from machining or polishing. This irregularities may allow gas to remain trapped. However given that the comparing pitted surface and finned surface has much larger irregularities, namely pits and fins, the microscopic pits and scratches can be ignored for comparison.



a) Pitted Surface

b) Plain Surface

c) Finned Surface

Fig. 3.2: Various types of surfaces used for experiment

3.4 Methodology

The following method was followed to carry out the research:

- i. A temperature resistant glass was placed on a circular stand. The stand was a combination of three legs and an upper circular plate containing a cut through for incorporating desired surface blocks. The circular plate had asbestos sheet glued on top of it to make sure that when the glass is placed, it makes a good seal. Moreover, to make sure the air tight sealing silicon glue was used to attach the glass with the plate. To hold the glass tight on its position, 4 long screws were used connecting bottom plate with a plate placed on top of the glass. The top plate also had a cut through for putting the block surface in its position.
- ii. The block surface was designed to prevent water leakage. A rubber ring band was attached on the top portion of the surface in a groove to make sure that when the surface come in

contact with the bottom plate, it makes a good seal. The tail of the block was covered with ebonite and screwed tightly to ensure air tightness as shown in Fig. 3.1

- iii. The tail of the block contained a channel to incorporate a cartridge heater having the heater top at the close proximity of the heating surface. The block was also drilled to have small holes to incorporate thermocouples.
- iv. A cartridge heater was placed in the block surface and connected with the variac.
- v. Distilled water was used. Water was poured into the glass container.
- vi. The high speed camera was placed facing the boiling setup. The camera was focused on the boiling surface. A computer was used to capture video from the camera, control the camera and play captured video of the camera.
- vii. As soon as the setup was ready, voltage was supplied to the heater using variac. Variac was adjusted by 5 Volts periodically up to 220 volts. The temperature reading was recorded from digital thermometer. The captured video was rendered to view-able video files for analysis.

3.5 Measurement Techniques

In this work, many test conditions were impossible to measure in a traditional manner. The high bubble departure speed, higher nucleation density and fluid motion made it hard to work out all required parameters in an efficient manner with higher accuracy. For example, precise time for the bubble departure was not precisely perceptible. On top of that, bubbles frequently merges. Bubble embryos gets attached to each other. While leaving the surface they pulled nearby bubbles which was still attached to the surface. In many cases they merged. The bubble that detaches from the surface has different diameter than a while later, when it merges with the attached embryo just after leaving the surface. This effectively changed the bubble departure diameter and made it hard to keep the consistency in diameter measurement. Moreover, some growing embryos moved from their nucleation site while still being attached to the surface and merged with neighboring bubble embryos. Even after leaving the surface the bubbles interacted with other bubbles while ascending. To keep the error at a minimal level, average of 10 bubble values is considered. Images of each bubble is traced from the beginning of the growth to the time they vanish. The pixels displacement of each of the bubbles was determined from separate frames. To make sure the diameter accuracy a reference millimeter scale was also used.

3.5.1 Bubble Departure Diameter

To calculate bubble departure diameter, from the high speed videos 5 frames were considered for each bubble from before and after the exact time of departure. The amount of pixels taken up by a bubble was measured along with each pixel size which provided the bubble diameter measurement. A millimeter scale was also used for reference. From Fig. 3.3 it can be seen that as soon as the bubble detached, it has lost its spherical shape and deformed. At this stage, the bubble departure diameter measurement could be erroneous. In Fig. 3.4 & Fig. 3.5 two merging bubble is observed. Merging two different bubble produces different diameter. Furthermore, some bubbles merge with neighboring bubble after detaching from surface. The diameter just before the departure is different than when it leaves the surface and merge with another bubble. At higher heat flux the bubbles formed at the surface are often irregular in shape and forms a longer bubble as shown in Fig 3.6 & 3.7.

These quirks contribute to considerable amount of scatter producing measurement uncertainty. It also obscures the definition of the key term “Bubble diameter”. The scatter occurs due to manual measurement of measuring non-spherical larger bubbles. The diameter reported in this work is based on the average equivalent diameter in normal surface view.

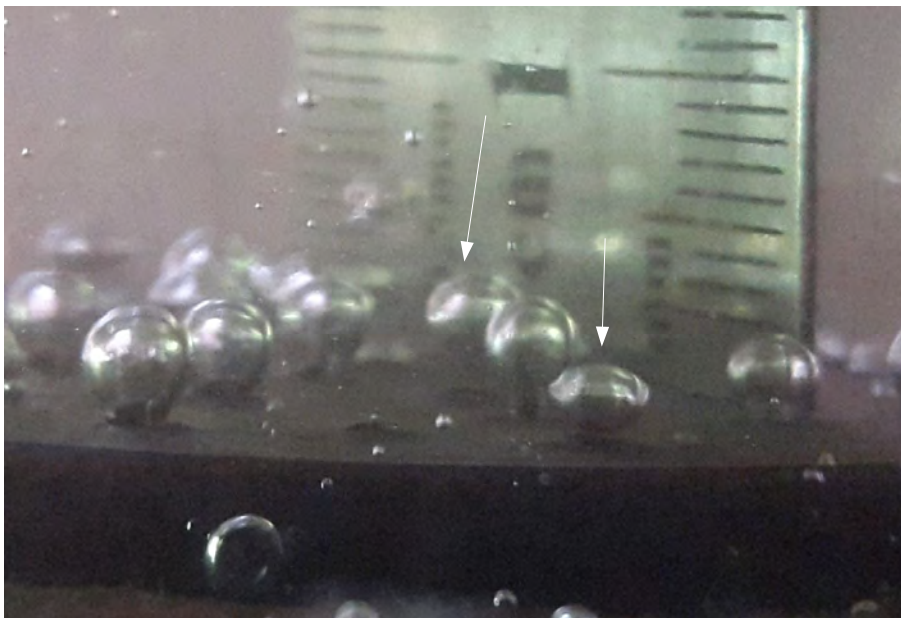


Fig. 3.3: Bubble deformation during detachment from surface [t=33 millisecond, ms]

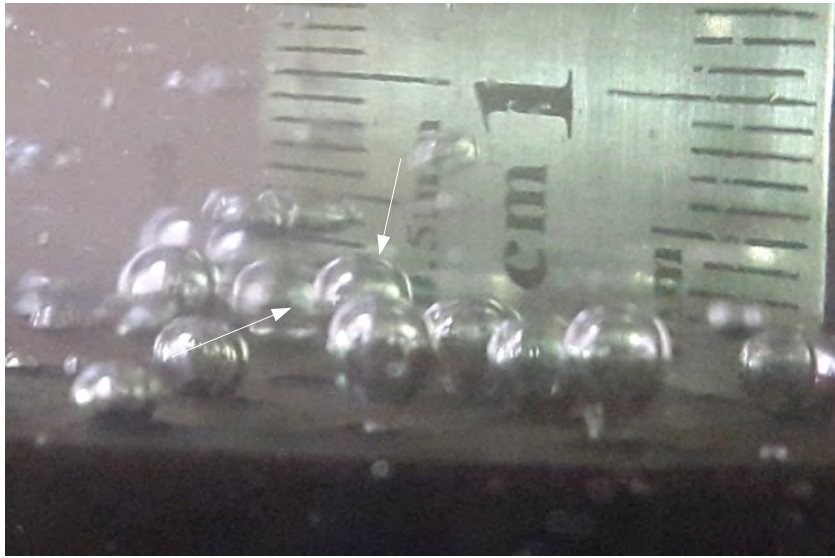


Fig. 3.4: Bubble merging before departure

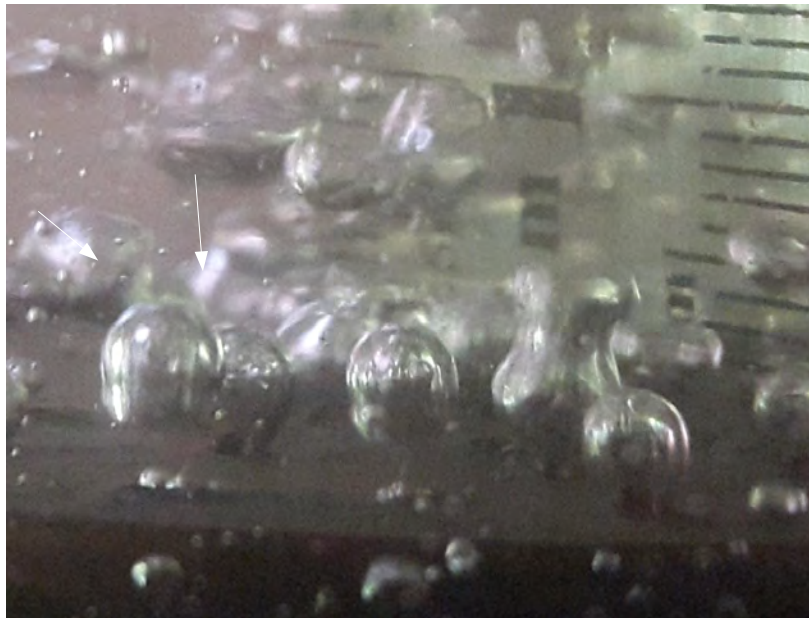


Fig. 3.5: Bubble merging while neighboring bubble is detached [t=35ms]

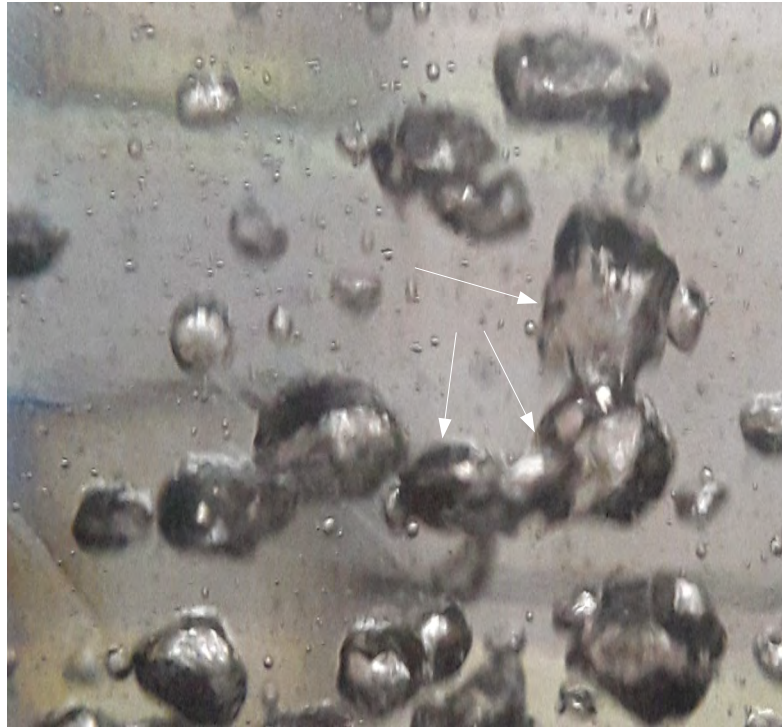


Fig. 3.6: Irregular shaped bubbles and merging at the ascend

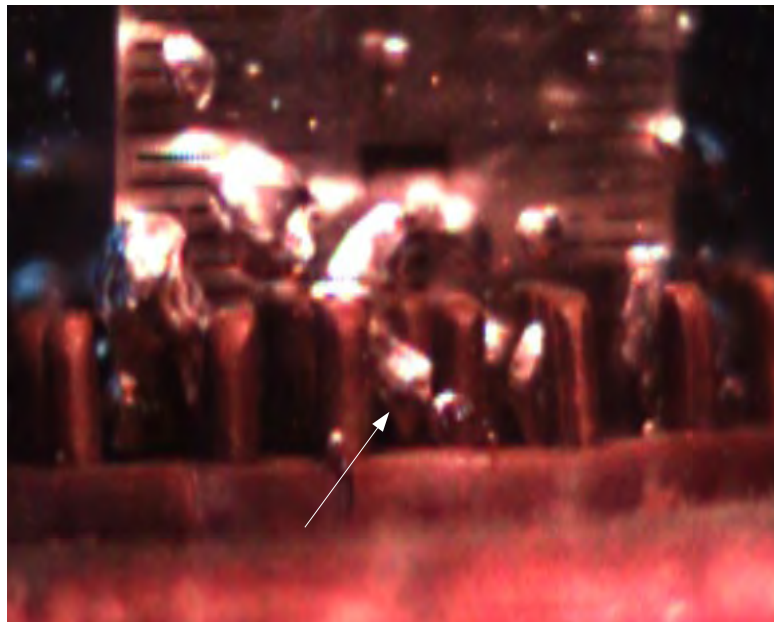


Fig. 3.7: Formation of irregular shaped bubbles at the surface

3.5.2 Bubble Departure Frequency

There are mainly two ways to determine bubble departure frequency [8]. One is proposed by Darby [22] which involves monitoring successive bubble formation on a single nucleation site and the difference in time. The other method simply take elapsed time into consideration between two bubble departure event. In this study, the frequency was determined from high speed video footage. Videos were analyzed frame by frame and the number of departing bubbles were recorded over a certain amount of time. Then the data were averaged over one second to determine departure frequency. In lower heat flux the bubble departure frequency is easier to determine. But at higher heat flux bubbles tends to merge frequently as shown in Fig. 3.6. The merging of two or more bubbles apparently makes it difficult to estimate the bubble departure frequency.

3.5.3 Wall-Temperature

To determine wall temperature thermocouple probes were used. Small drills were made on the test pieces half a millimeter below the top surface. The type of the thermocouple were K-Type. A digital thermometer was attached to the other end of the probe and was calibrated to reflect actual temperature of the surface.

3.5.4 Heat Flux

Heat flux is calculated using the following equation:

$$\text{Heat flux, } q = (V I \cos\theta - q_L)/A$$

where,

V = Voltmeter reading, Volt

I = Clip-on multi-meter reading, ampere

$\cos\theta$ = Power factor, 0.85

q_L = Heat loss from the heater assembly

A = Cross sectional area of boiling surface, m^2

Wall superheat is calculated using the following relation:

$$\Delta T = T_w - T_{sat}$$

where,

T_w = Temperature of boiling wall surface.

T_{sat} = Saturation temperature of the working fluid.

Boiling heat transfer coefficient, h was also calculated using the following relation:

$$h = q / \Delta T$$

Chapter 4.

RESULT & DISCUSSION

One of the measured parameters of the study is heat flux which is the actual controller of pool boiling. The other measured parameters include bubble departure diameter, bubble departure frequency, heat transfer coefficient and wall superheat. In this chapter, their characteristics and inter-relation will be discussed.

4.1 Bubble Departure Diameter

The bubble departure diameter was measured with the help of still images from the high speed video. The final diameter was obtained from an average of at least 5 bubbles' diameter. The bubble departure diameter for plain surface with respect to heat flux is shown in Fig. 4.1.

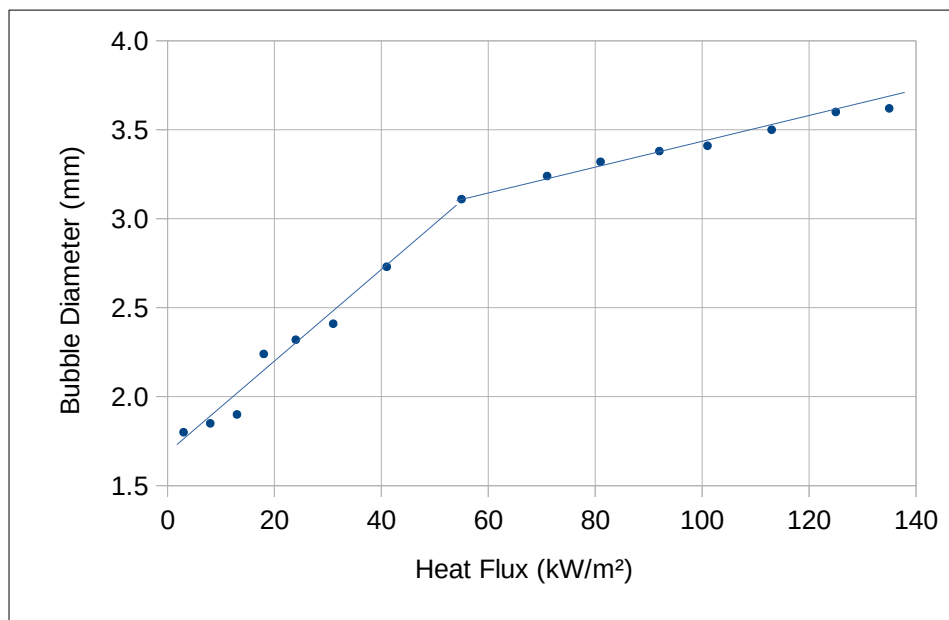


Fig. 4.1: Variation of bubble departure diameter with the increase of heat flux on plain surface.

From the figure it is seen that the bubble departure diameter increases with the increase of heat flux. However, the initial rate of increase of bubble departure diameter is higher up to the heat flux value

of 60 kW/m^2 . At the start of the boiling the bubble count is lower and the nucleation sites are few. Bubbles are more stable at this time. The less bubbles hardly disturbs the fluid resulting less fluid motion. Bubble also forms keeping considerable distance between them as well as between each nucleation site. As a result the acting forces on each bubble is much less which let the bubbles take up the heat from the surface for longer period without detaching as shown in Fig. 4.2.

The prolonged heat absorption by the bubble while still attached to the surface let the bubble grow in relatively larger sizes. With the increase of heat flux, the nucleation sites start to increase as well as the bubble count. Hence increases the bubble departure frequency. As soon as the bubble departure frequency increases, the fluid motion changes drastically. This changes the stability of bubbles and working fluid.



Initialization of a bubble embryo [t=3ms]



Prolonged heat absorption and growth [t=120ms]



Detachment from the surface [t=130ms]

Fig. 4.2: Birth, growth due to prolonged heat absorption and detachment of a bubble

The bubbles get comparatively less time to stick to the surface due to fluid motion. Unlike previously when the bubbles used to grow generally isolated from each other, the increase in the number of bubble formation changes that scenario. Often two or more bubbles tend to grow from the same site and their embryos remain attached to each other. The larger bubble slides away from the pairing exerting a sliding force on the smaller bubble in the direction of bulk fluid flow. Some bubbles merge with each other before leaving the surface originating from the same site. This affects the average bubble departure diameter. On the other hand, at higher heat flux, the inertia of bubbles becomes important [9].



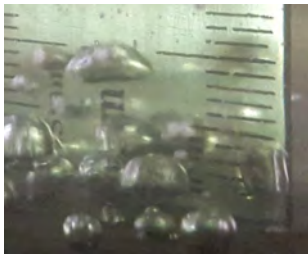






For fluid motion in boiling, it is assumed that the bubble detaches if the combination of buoyancy and drag force is able to overcome the force due to surface tension [23]. Along with the bulk liquid flow direction the drag force includes the quasi-steady drag. It also incorporates unsteady drag due to the asymmetric growth of the bubble inclined in the direction of the liquid flow as well as the shear lift force. Bubbles can detach in both parallel and normal in respect to the heating surface. It has been observed that at higher heat flux, most often the bubbles slide away over the heating surface before it can lift off into the bulk liquid.

This, however, might imply that surface tension alone is not responsible for keeping the bubble attached to the surface. The drag force acting on the bubble due to the asymmetrical growth of bubbles and active force opposite to the fluid flow may also be responsible for bubbles to remain attached to the surface. On the other hand with the increase of wall superheat the rate of heat transfer into the vapor bubble increases. Hence, bubble diameter increases in the second part of the trend line but it is less steep than the first part as shown in Fig. 4.1.

Table 4.1 shows bubble departure phenomena at different heat flux. For the plain surface, at lower heat flux up to 10 kW/m^2 the bubble forms a complete bubble embryo. The nucleation sites are fewer at this stage. But with the increase of heat flux, the bubble number increases as well as nucleation site densities. It is also observed that at higher heat flux the departed bubble's shape deforms and the bubble departure frequency increases.

For the pitted and finned surface, it is observed that the number of nucleation site is higher in lower heat flux than the plain surface. Both bubble departure diameter and bubble departure frequencies are higher at $q = 60 \text{ kW/m}^2$ for pitted and finned surface. With pitted and finned surface, at $q = 120 \text{ kW/m}^2$ bubbles frequently merges and forms larger bubbles than the plain surface.

Table 4.1: Visuals of bubbles on different surface at different heat flux level

Surface Type\Heat Flux	$q = 10 \text{ kW/m}^2$	$q = 60 \text{ kW/m}^2$	$q = 120 \text{ kW/m}^2$
Plain Surface			
Pitted Surface			
Finned Surface			

The average bubble departure diameter was compared against the correlation given by Hamzekhiani et. al. [6], which is shown in Fig. 4.3.

From Fig. 4.3 it is seen that the present experimental bubble departure diameter trend with heat flux is comparable with Hamzekhiani et. al.'s [6] predictive correlation data. Two different type of enhanced surfaces have been compared with the plain surface, one is pitted surface and the other is finned surface in the present study. As shown in Fig. 4.4 at the beginning, the average bubble departure diameter is slightly higher at the pitted surface compared to the plain surface. This is

because air remain trapped in the pits and starts forming expanding bubble embryos as soon as the heat is supplied. 20, 25 and 30 pits' surface have been tested as shown in Fig. 4.4.

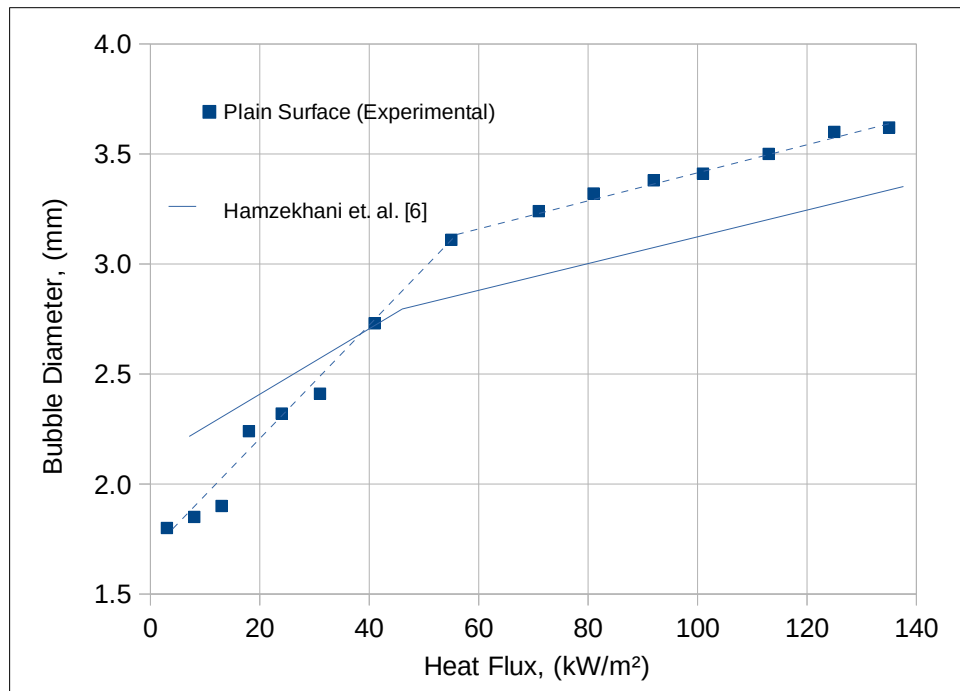


Fig. 4.3: Variation of bubble departure diameter with respect to heat flux, compared with Hamzekhani's [6] predictive correlation.

Like plain surface, no regular behavior is observed in pitted surface. Bubble embryos are hardly isolated at the beginning in pitted surface. Which result in frequent merging of bubbles with neighboring bubbles. Also the active site densities are higher in number, which all contributes to the higher bubble departure diameter compared to plain surface, as shown in Fig. 4.4. It is observed that often bubbles merges with each other and form a single bubble before departure. It's difficult to predict the behavior of how often and how frequently it happens.

Finned surface shows a different pattern than plain and pitted surface. The bubble departure diameter at the beginning of boiling is larger than both plain and pitted surface. Which may be the result of initial higher heat transfer by the fins and trapped gas. At the very beginning, the fluid motion is quite steady and stable. The bubbles formed in this stage can absorb more heat without fluid motion pushing on it. Which in turns let the bubbles grow. But as soon as the bubbles start to leave the surface in large number with the increase of heat flux, the fluid motion scatters them. The process is more accelerated compared to plain and pitted surface.

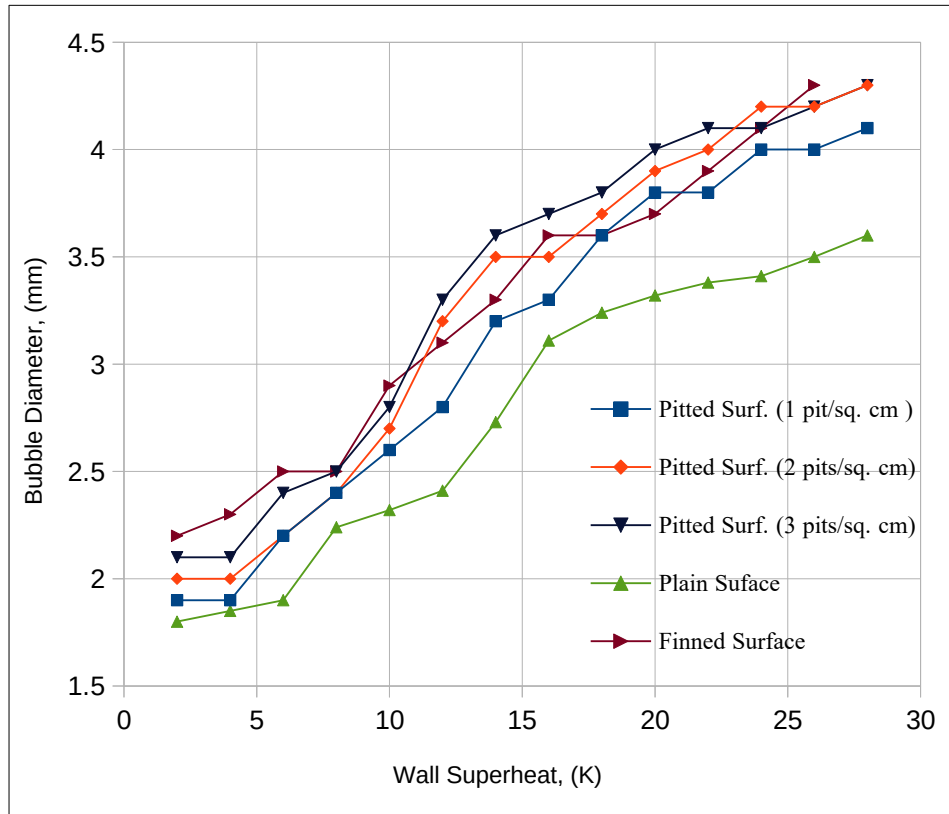


Fig. 4.4: Comparison of different surfaces' bubble diameter with respect to wall superheat.

From Fig. 4.4 it is observed that after the initial heat transfer the average bubble departure diameter for finned surface becomes less compared to average pitted surface's bubble departure diameter. But the heat transfer coefficient is higher in finned surface despite average bubble diameter being shrunken. The phenomena occur because higher heat flux produces high bubble departure frequency allowing high heat transfer. It is evident that not only bubble departure diameter affects heat transfer, but also bubble departure frequency plays an important role. The reduction in heat transfer could have happened with the decreased bubble departure diameter, but higher bubble departure frequency compensated for the bubble departure diameter.

4.2 Bubble Departure Frequency

Bubble departure frequency is plotted in the Fig. 4.5 against wall superheat for all the three surfaces. As a general notion, it is seen from the plot that with the rise of wall superheat the rate of bubble departure increased for all surfaces. However, bubble departure frequency is significantly higher for finned and pitted surface compared to the plain surface.

When Fig. 4.5 is compared with Fig. 4.6, it is found that in general higher bubble departure frequency is linked to higher heat flux. It has been observed that higher heat flux increases nucleation sites. Nucleation sites are responsible for producing bubbles. As more nucleation sites are formed the more bubbles are formed and released from the surface. This is why higher wall superheat as well as higher heat flux tend to increase bubble departure frequency. When the bubble departure frequency increases, the bubbles scatter randomly due to fluid motion while ascending. This allows bubbles to collide with each other more often. As a result bubbles frequently merge and form vapor columns, central bubble column and bubble mushroom-cloud.

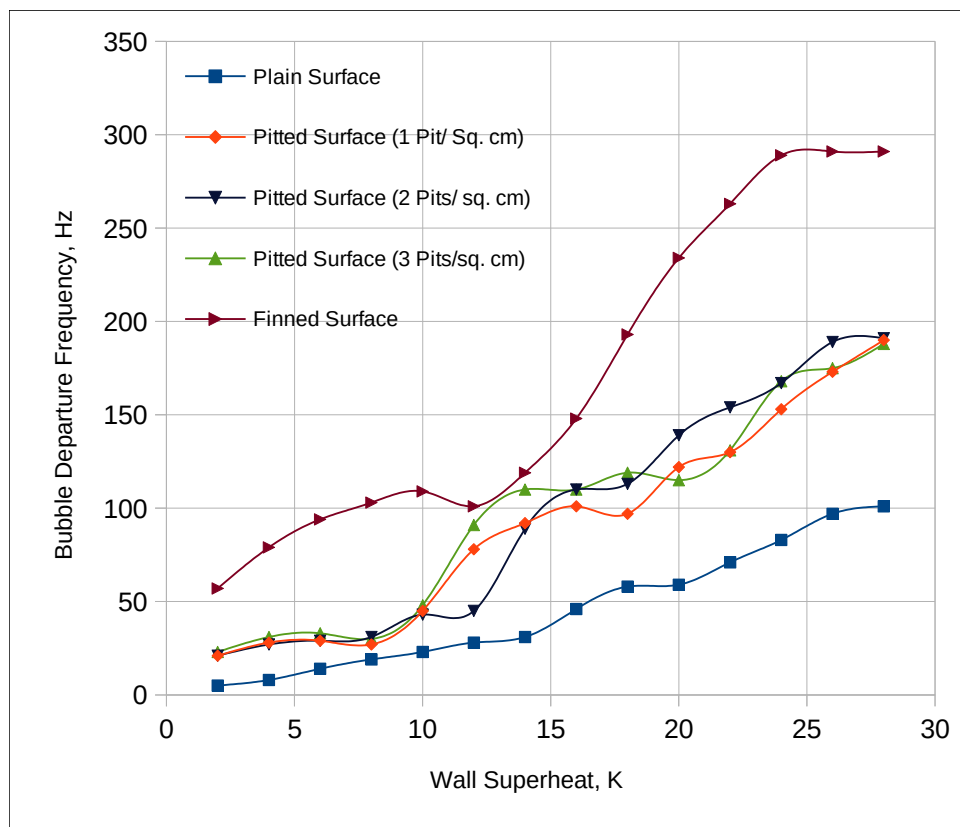


Fig. 4.5: Bubble departure frequency at different heat flux

For lower and mid range heat fluxes the bubble merging and ascending is irregular and isolated to their own nucleation sites. Lower heat flux result in fewer nucleation sites, which is why the bubbles merge with next bubble in their own nucleation sites.

At the wall surface, larger bubbles are visible which are formed by merging bubbles with each other. In lower heat flux, bubbles usually merge with the next bubble on the same site. Sometime a second bubble forms as soon as the first bubble completes its growth. Two bubbles coincide at same site while one bubble is fully grown and the other is just halfway through the growth. In this case, two bubbles merge in the vertical direction rather than horizontal. As a result, the lower portion of the merged bubble springs up due to the restoring action of the surface tension force. When three or four successive bubbles merge, a mushroom type vapor bubble is formed.

With the increase of heat flux nucleation sites also increases and bubbles merge with other bubbles of different nucleation site. It let the bubbles from all the nucleation sites to form a central buoyant bubble column and merges with each other while ascending to the top layer of the fluid surface. This enables bubbles to merge with bubbles from different nucleation site. This happens rapidly. It also makes it possible for the bubbles to depart in higher frequency on the pitted and finned surface than the plain surface as shown in Fig. 4.5. In Fig. 4.6, Fig. 4.7, Fig 4.8 wallsuperheat is compared with corresponding heat flux for all three different surfaces.

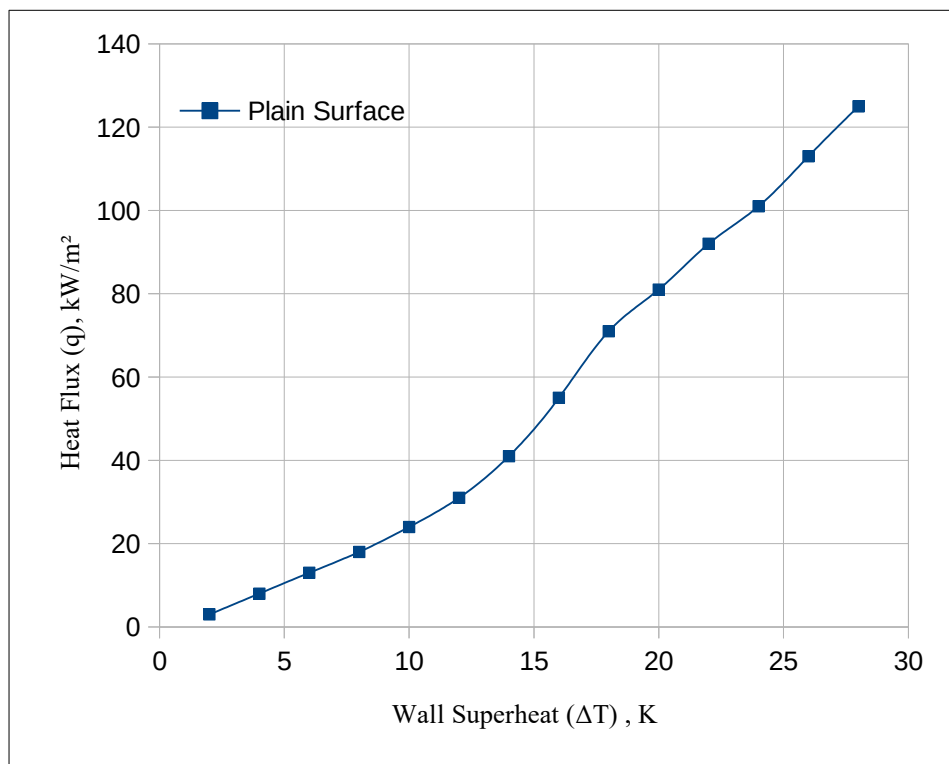


Fig. 4.6: Wall superheat vs. heat flux plot for plain surfaces

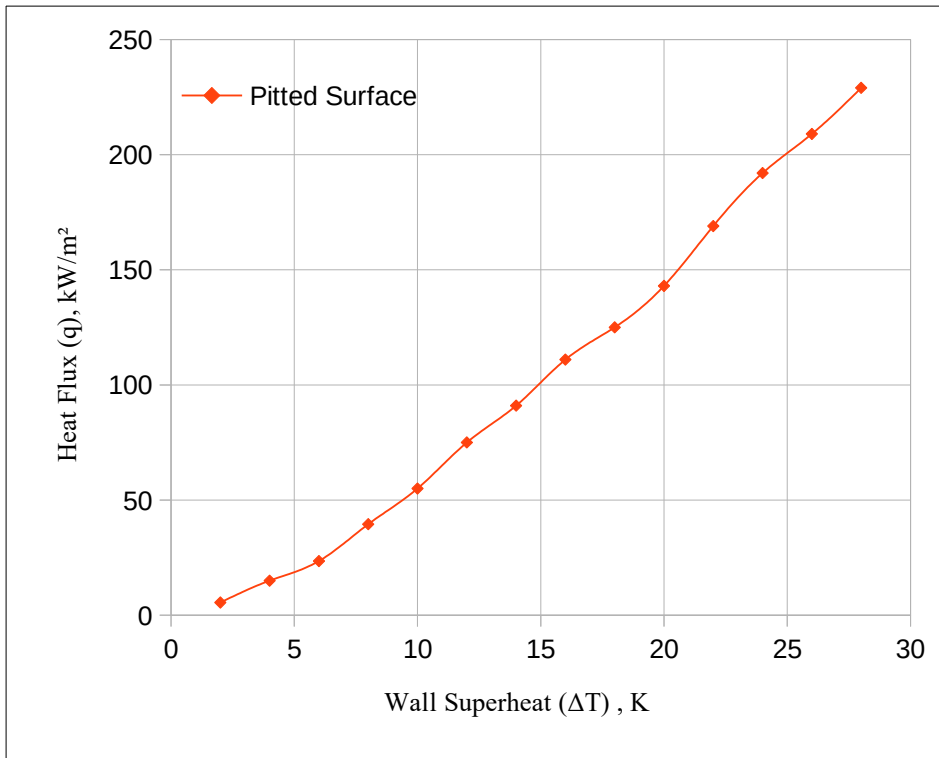


Fig. 4.7: Wall superheat vs. heat flux plot for pitted surfaces

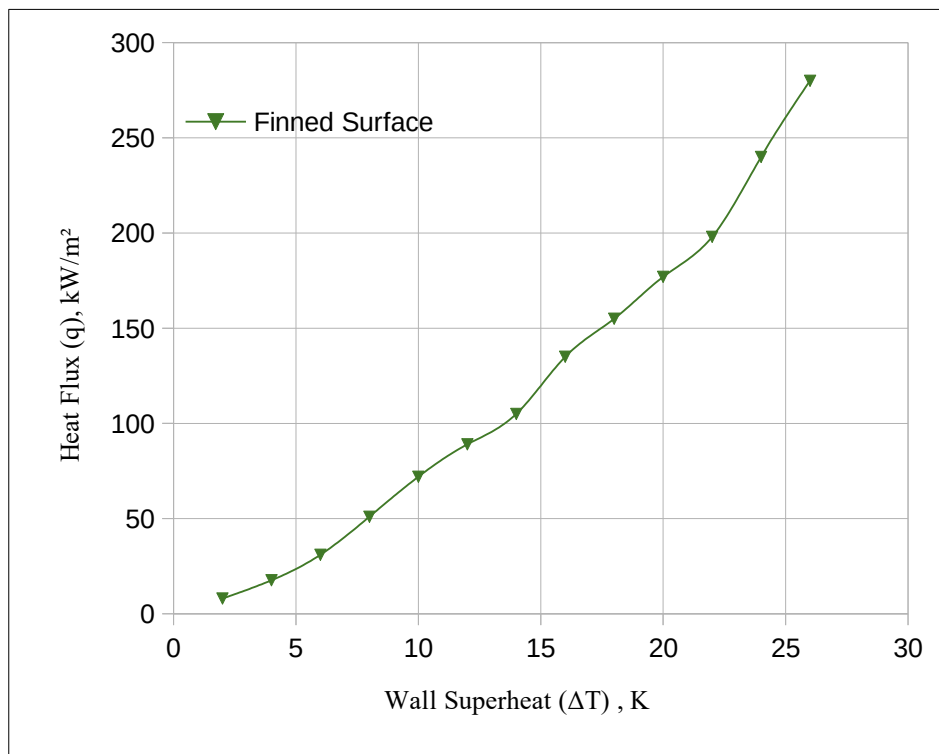


Fig. 4.8: Wall superheat vs. heat flux plot for finned surfaces

From Fig. 4.5 it is observed that for finned surface bubble departure frequency dropped after initial bubble release. This might happen because the bubble merging couldn't be accomplished as freely as it did on the pitted and plain surface. Fins may have acted as a barrier for merging different site's bubbles on the surface. Fins also restrained bubbles from merging with neighboring bubbles at the surface, resulting smaller bubbles compared to pitted surface. As soon as the heat flux increased the bubble departure frequency started to increase and formed buoyant column and bubble cloud.



Fig. 4.9: Image obtained at 70 kW/m² on pitted surface showing the formation of buoyant column

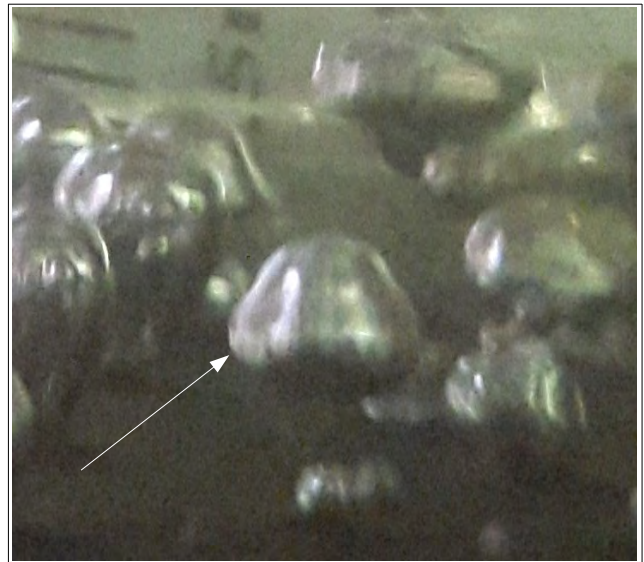


Fig. 4.10: Mushroom type vapor bubble formed by bubble merging

A buoyant column formation is shown in Fig. 4.9 and a mushroom type vapor bubble is shown in Fig. 4.10. In Fig. 4.11 a typical onsite bubble merging is shown. Various studies involves linking frequency (f) with bubble departure diameter(D). Jakob and Linke [24] and Rohsenow [13] both have presented the analysis linking frequency and bubble departure diameter. The product of fD^3 is also used in critical heat flux analysis using liquid continuous-vapor discontinuous model [25].

Jakob and Fritz [26] proposed that the product of frequency and departure diameter should be a constant, regardless of other conditions. But the correlation developed by Jakob and Fritz [26] was based on experimental data acquired from the pool boiling of water and liquid hydrogen. None of the previous correlations show any similarities with current experimental data. In this study, both the departure diameter and departure frequency of bubble were observed to increase with increase of heat flux and wall superheat.

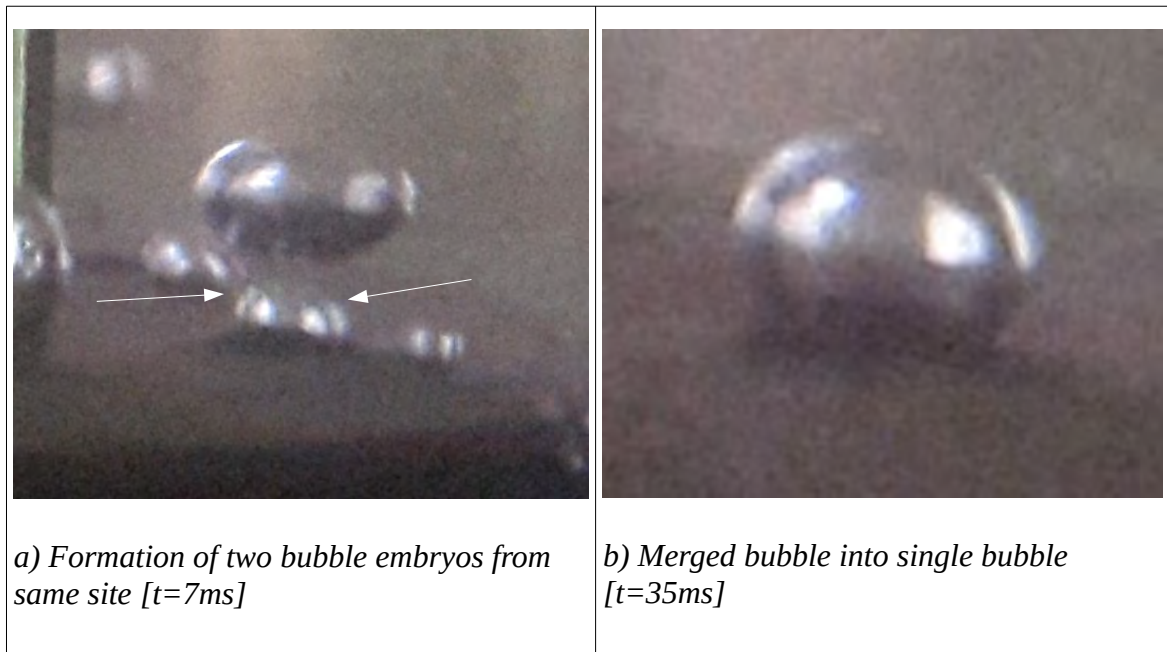


Fig. 4.11: Merging of bubbles in same site

4.3 Heat Transfer

Wall superheat and respective heat transfer coefficient is plotted in the Fig. 4.12 as well as heat flux and respective heat transfer coefficient is plotted in the Fig. 4.13. It is evident that surface topography has dramatic influence on the heat transfer process. Both finned and pitted surface has significantly higher heat transfer coefficient than plain surface. It is also observed that increasing cavities lead to an increase of heat transfer coefficient. In surfaces with 1 pit/cm², 2 pit/cm², and 3 pit/cm², they have slightly varied heat transfer coefficient. The pitted surface promotes the heterogeneous nucleation and increases nucleation site. In finned surface, the heat transfer coefficient is even higher. From Fig. 4.12 it has also been observed that after a steeper increase in heat transfer coefficient the rate of increase of heat transfer coefficient drops. This phenomena is more noticeable in finned surface. When Fig. 4.12 is compared with Fig. 4.5 and Fig. 4.4, it can be observed that at this period both bubble departure frequency and bubble departure diameter dropped slightly. Which might have caused the heat transfer coefficient to be less than desired. The heat transfer coefficient curve for finned and plain surface is also less steeper compared to the earlier trend. This might be the result of bubble coalescence. At high heat flux horizontal bubble merging occurs frequently as shown in Fig. 4.14.

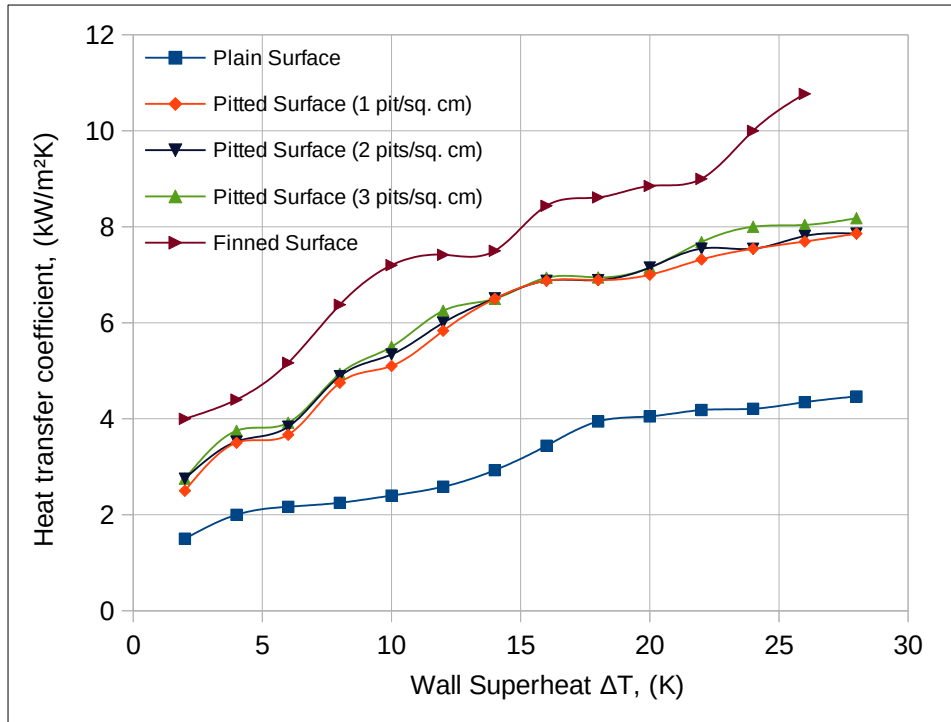


Fig. 4.12: Heat transfer coefficient at different wall superheat for different surfaces

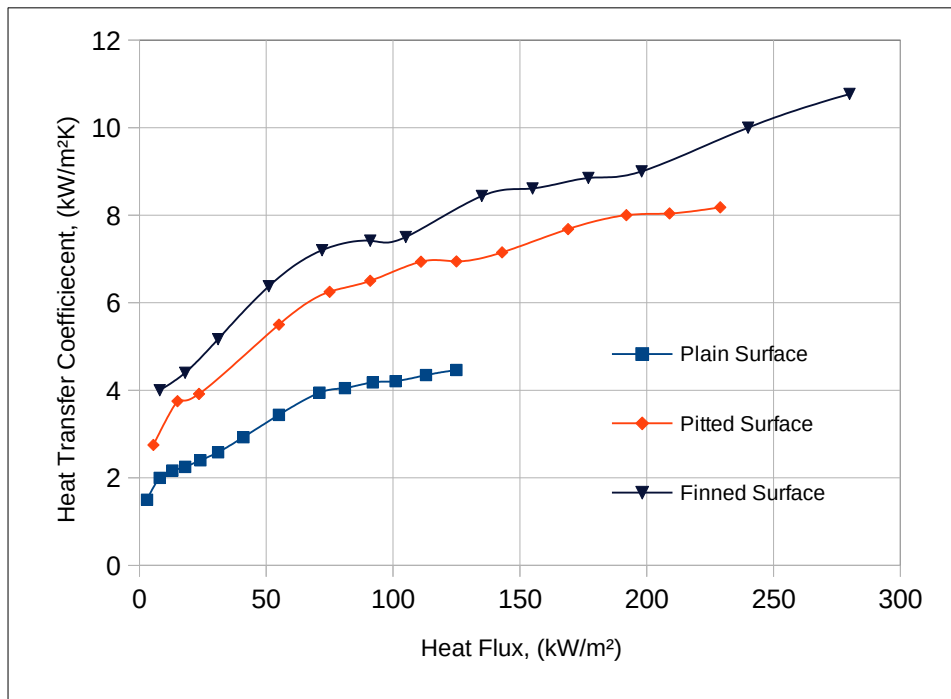
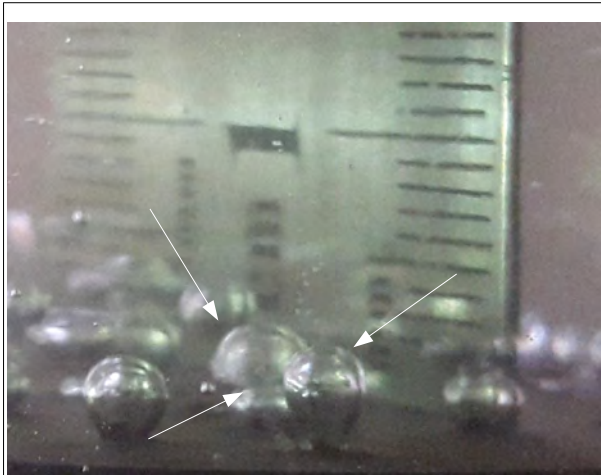
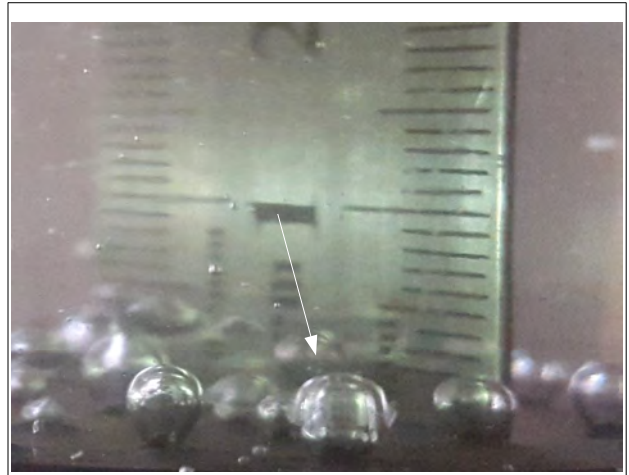


Fig. 4.13: Heat transfer coefficient at different heat flux level for different surfaces



[t=80ms]



[t=110ms]

Fig. 4.14: Merging of 3 bubble embryos into one in plain surface

Chapter 5.

DEVELOPMENT OF CORRELATION

A mathematical correlation based on dynamic bubble behavior is very complicated and difficult to achieve. As the variables increase the mathematical terms starts to be more complicated. For the complexity of the bubble departure phenomena, a fully theoretical predictive model has not yet been possible to develop. To minimize the limitation, several influencing parameters have been considered for developing the mathematical predictive model i.e. bubble diameter, bubble departure frequency, surface tension, acceleration of gravity, heat flux, and vapor-liquid density difference. Bubble departure diameter is considered as a function of heat flux, vapor-liquid density difference, gravity, latent heat of vaporization and surface tension. Mathematically this can be expressed as follows:

$$d = f(q, \Delta\rho, g, \sigma, h_{fg})$$

The characteristic dimension $L_c = \sqrt{\frac{\sigma}{g(\rho_l - \rho_v)}}$ is widely considered for pool boiling. It is known to be proportional to the bubble departure diameter and to the dimension of the thermal boundary layer [27]. Assessing the criteria for π -grouping, two groups are formed. The first π group represents dimensionless number which measures the effect of gravitational forces with respect to surface tension and is used to represent the shape of bubble surrounding in fluid.

$$\text{First } \pi \text{ group, } \pi_1 = d \sqrt{\frac{(\rho_l - \rho_v)g}{\sigma}}$$

The Eotvos or Bond number is expressed as $Bo = \frac{\Delta\rho g L^2}{\sigma}$. First π term can be expressed in terms of Bond number, as characteristic dimension L is proportional to bubble diameter d.

On the other hand, the supplied heat flux during boiling is one of the dominant factor in pool boiling represented by the second pie group.

Second π group, $\pi_2 = \frac{q}{\sqrt[4]{(\rho_l - \rho_v)g^3 \sigma^3}}$

Third π group, $\pi_3 = h_{fg} \sqrt{\frac{(\rho_l - \rho_v)}{g \sigma}}$

Once all the π groups are formed, new correlation proposed for pool boiling can be rearranged in the following form:

$$d \sqrt{\left(\frac{(\rho_l - \rho_v)g}{\sigma}\right)} = C \left[\frac{q}{\sqrt[4]{(\rho_l - \rho_v)g^3 \sigma^3}} \right]^a \left[h_{fg} \sqrt{\frac{(\rho_l - \rho_v)}{g \sigma}} \right]^b \quad (5)$$

Here C is a constant and 'a' and 'b' are fitting parameters. After regression analysis, for different surfaces the fitting parameters are a=0.23 and b=1 and C=1.5×10⁻⁹. The final equation is presented below with fitting parameters:

$$d \sqrt{\left(\frac{(\rho_l - \rho_v)g}{\sigma}\right)} = 1.5 \times 10^{-9} \left[h_{fg} \sqrt{\frac{(\rho_l - \rho_v)}{g \sigma}} \right] \left[\frac{q}{\sqrt[4]{(\rho_l - \rho_v)g^3 \sigma^3}} \right]^{0.23} \quad (6)$$

For simplicity, surface roughness, atmospheric pressure, surface geometry, pitted surface's cavity depth, fin lengths were not considered.

To compare the experimentally acquired data with the proposed correlation absolute average error was calculated with the following equation:

$$AAE \% = \left| \frac{d_{predict}}{d_{experimental}} - 1 \right| * 100 \quad (7)$$

For visual comparison the data for experimental bubble diameter were plotted against bubble diameter acquired from proposed correlation in Fig. 5.1 for plain surface. It is observed in the plot that with the increase of bubble diameter the predicted values become more accurate. This trend is also repeated for pitted and finned surface as shown respectively in Fig. 5.2 and Fig. 5.3.

With this new proposed empirical correlation the error rate is significantly lower. Table 5.1 shows the percentage of absolute average error between experimental data and proposed correlation.

Table 5.1: Error rate of proposed empirical correlation with respect to experimentally obtained results:

Surface Type:	Plain Surface	Pitted Surface	Finned Surface
Error Rate:	9%	6%	12%

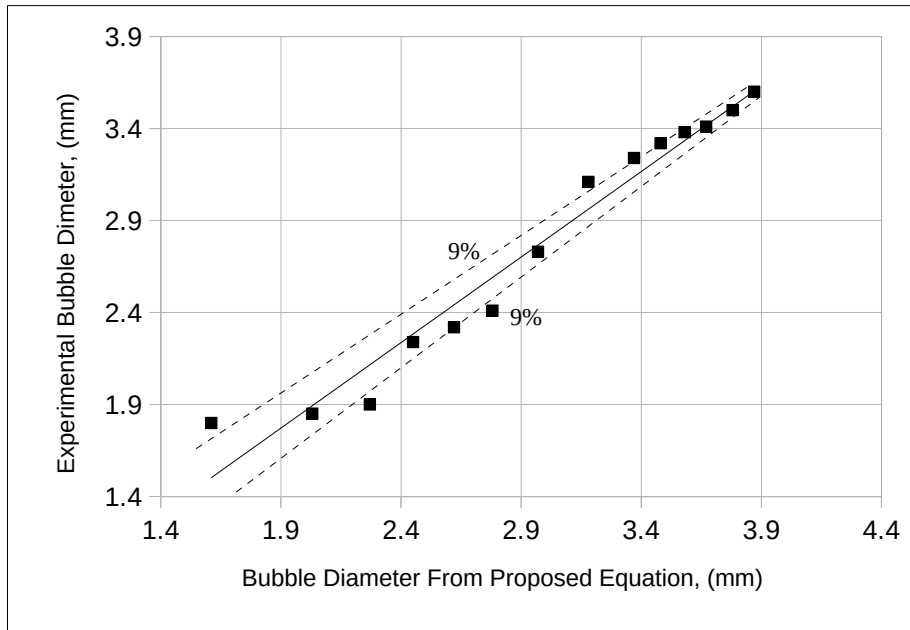


Fig. 5.1: Bubble diameter from proposed equation vs. experimental bubble diameter for plain surface

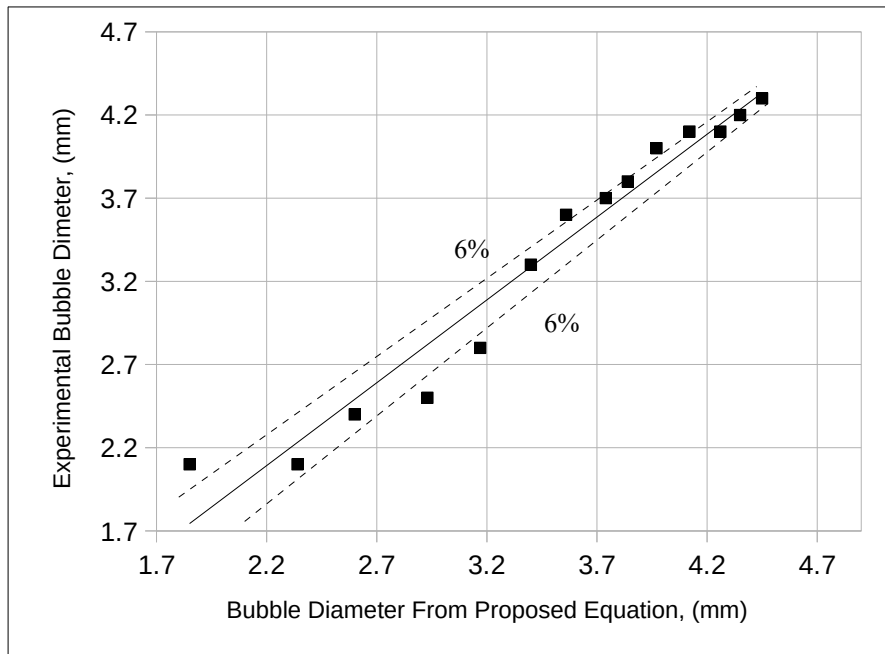


Fig. 5.2: Bubble diameter from proposed equation vs. experimental bubble diameter for Pitted surface

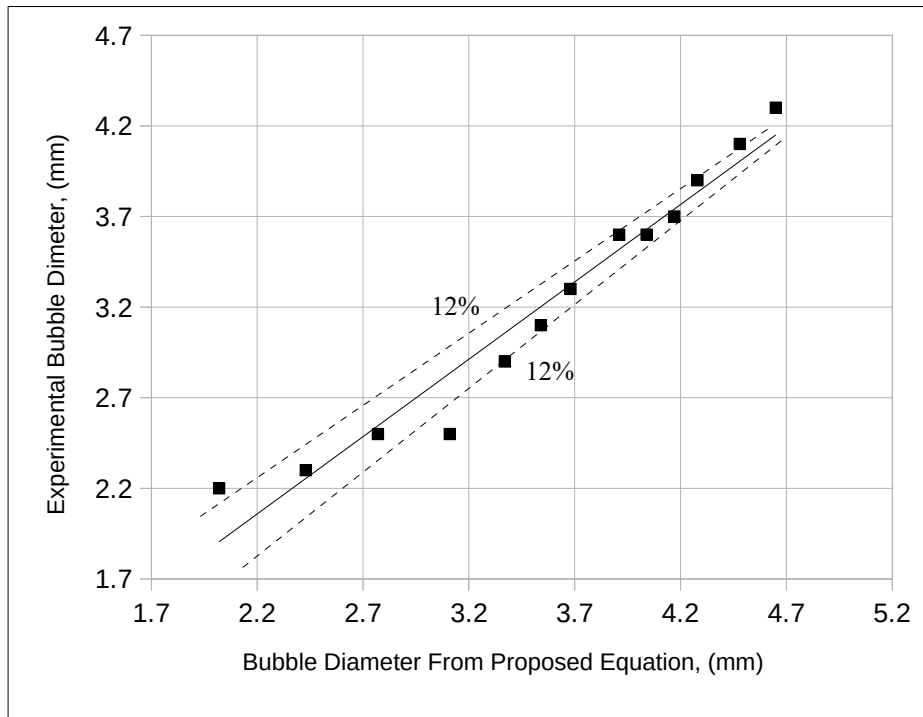


Fig. 5.3: Bubble diameter from proposed equation vs. experimental bubble diameter for Finned surface

Chapter 6.

CONCLUSION & RECOMMENDATION

An experimental and a theoretical study have been carried out to investigate the true nature of bubble dynamics in pool boiling. Results of the experiment has been well documented and analyzed in the previous chapters. A summary of the findings and future recommendation is enlisted in this chapter.

6.1 Conclusion

In this study, the relation among the bubble departure diameter, bubble departure frequency and heat transfer in pool boiling on different surface topography is studied. In this section, conclusion is drawn based on the experimental findings. Summary of the conclusion is listed below.

- It has been observed that with the increase of heat flux the bubble departure diameter increases for all types of surfaces. This incorporates higher heat transfer.
- Along with heat flux, surface roughness also plays an important role in bubble departure diameter. The bubble departure diameter on the pitted surface is significantly higher than plain surface as well as the bubble departure frequency.
- Bubble departure frequency is higher for the finned surface. It has been also observed that heat transfer coefficient is also higher for the finned surface which leads to the conclusion that bubble departure frequency has effects on heat transfer.
- Bubble merging in pool boiling has significant effect on crucial pool boiling parameters i.e. bubble diameter, bubble departure frequency and heat transfer coefficient.
- Heat transfer coefficient increases with the increase of heat flux for all surfaces.
- Heat transfer coefficient and bubble departure frequency is significantly higher for finned and pitted surface compared to the plain surface.
- The experimental data from the present study has well agreed with literature.
- Based on the experimental data, an empirical correlation has been proposed with reasonable agreement (Error: 10%) with the present experimental data for all of the three surfaces.

6.2 Recommendation

With each study and research a small boundary is pushed towards better understanding of a science and engineering problem. At the same time, it also opens a lot of opportunity for future research.

Based on the present experiment following recommendations can be made:

- The experimental result showed that modified surface enhances pool boiling phenomena. More prominent surface modification can be designed to further enhance the pool boiling
- It has been observed that for the pitted surface, increasing the number of pits contribute to higher heat transfer rate. A comprehensive study can be carried out about how pit depth and number of pits on the surface is affecting the pool boiling phenomena.
- Wide range of fin size can be used to enhance the pool boiling. In this experiment round fins have been used. Different types of fin design can be studied to investigate the effect of topography of fin design on pool boiling.
- Fluid and bubble velocity can be taken into consideration for future investigation. It has been observed that fluid and bubble velocity may have effects on the pool boiling phenomena.
- The experiment can be carried out in different pressure other than atmospheric pressure to investigate how different pressure level affects the pool boiling phenomena.
- Different liquid can be considered for future research.
- More controlled surface modification can be done.

REFERENCE

- [1] Lord Rayleigh, "On the pressure developed in a liquid during the collapse of a spherical cavity," *Lond. Edinb. Dublin Philos. Mag. J. Sci.*, vol. 34, no. 200, pp. 94–98, Aug. 1917.
- [2] S. A. Alavi Fazel and S. B. Shafaei, "Bubble Dynamics for Nucleate Pool Boiling of Electrolyte Solutions," *J. Heat Transf.*, vol. 132, no. 8, p. 081502, 2010.
- [3] W. Fritz, "Berechnung des Maximal volumens von Dampfblasen," 1935.
- [4] E. Ruckenstein, "A physical model for nucleate boiling heat transfer," *Int. J. Heat Mass Transf.*, vol. 7, no. 2, pp. 191–198, 1964.
- [5] S. J. D. Van Stralen and W. Zijl, "Fundamental developments in bubble dynamics," *Proc. Sixth Int. Heat Transf. Conf.*, no. 6, pp. 429–450, 1978.
- [6] S. Hamzekhani *et al.*, "Bubble dynamics for nucleate pool boiling of water, ethanol and methanol pure liquids under the atmospheric pressure," *J. Appl. Fluid Mech.*, vol. 8, no. 4, pp. 893–898, 2015.
- [7] S. M. Peyghambarzadeh, A. Hatami, A. Ebrahimi, and A. Fazel, "Photographic study of bubble departure diameter in saturated pool boiling to electrolyte solutions," *Chem. Ind. Chem. Eng. Q.*, vol. 20, no. 1, pp. 143–153, 2014.
- [8] J. P. McHale and S. V. Garimella, "Bubble nucleation characteristics in pool boiling of a wetting liquid on smooth and rough surfaces," *Int. J. Multiph. Flow*, vol. 36, no. 4, pp. 249–260, 2010.
- [9] D. Gorenflo, U. Chandra, S. Kotthoff, and A. Luke, "Influence of thermophysical properties on pool boiling heat transfer of refrigerants," *Int. J. Refrig.*, vol. 27, no. 5, pp. 492–502, Aug. 2004.
- [10] S. Nukiyama, "The maximum and minimum values of the heat Q transmitted from metal to boiling water under atmospheric pressure," *Int J Heat Mass Transf.*, vol. 27, no. 7, pp. 959–970, 1984.
- [11] K. Stephan and M. Abdelsalam, "Heat-transfer correlations for natural convection boiling," *Int. J. Heat Mass Transf.*, vol. 23, no. 1, pp. 73–87, 1980.
- [12] R. Cole and W. M. Rohsenow, "Correlation of Bubble Departure Diameters for Boiling of Saturated Liquids," presented at the National Heat Transfer Conference, 1968.
- [13] W. M. Rohsenow, "A method of correlating heat transfer data for surface boiling of liquids," Cambridge, Mass.: MIT Division of Industrial Cooperation,[1951], 1951.

- [14] B. B. Mikic and W. M. Rohsenow, "A New Correlation of Pool-Boiling Data Including the Effect of Heating Surface Characteristics," *J. Heat Transf.*, vol. 91, no. 2, p. 245, 1969.
- [15] A. K. Mozumder and M. M. Kamal, "THERMO-VISUAL INVESTIGATION OF A TWO-PHASE CLOSED LOOP THERMOSYPHON," *Int. J. Mech. Mater. Eng. IJMME*, vol. 6, no. 1, pp. 109–119, 2011.
- [16] G. Leppert, "BOILING HEAT TRANSFER," *J. Am. Soc. Nav. Eng.*, vol. 73, no. 2, pp. 331–340, Mar. 2009.
- [17] H. Chi-Yeh and P. Griffith, "The mechanism of heat transfer in nucleate pool boiling—Part I," *Int. J. Heat Mass Transf.*, vol. 8, no. 6, pp. 887–904, Jun. 1965.
- [18] T. H. K. Frederking and D. J. Daniels, "The Relation Between Bubble Diameter and Frequency of Removal From a Sphere During Film Boiling," *J. Heat Transf.*, vol. 88, no. 1, p. 87, 1966.
- [19] S. A. Alavi Fazel and S. B. Shafaei, "Bubble Dynamics for Nucleate Pool Boiling of Electrolyte Solutions," *J. Heat Transf.*, vol. 132, no. 8, p. 081502, 2010.
- [20] A. Luke, "Interactions between bubble formation and heating surface in nucleate boiling," *Exp. Therm. Fluid Sci.*, vol. 35, no. 5, pp. 753–761, 2011.
- [21] I.-C. Chu, H. C. No, and C.-H. Song, "Bubble Lift-off Diameter and Nucleation Frequency in Vertical Subcooled Boiling Flow," *J. Nucl. Sci. Technol.*, vol. 48, no. 6, pp. 936–949, Jun. 2011.
- [22] R. Darby, "The dynamics of vapour bubbles in nucleate boiling," *Chem. Eng. Sci.*, vol. 19, no. 1, pp. 39–49, 1964.
- [23] V. K. Dhir, H. S. Abarajith, and D. Li, "Bubble Dynamics and Heat Transfer during Pool and Flow Boiling," *Heat Transf. Eng.*, vol. 28, no. 7, pp. 608–624, Jul. 2007.
- [24] M. Jakob and W. Linke, *Heat Transfer*, vol. 1. New York: John Wiley, 1949.
- [25] H. J. Ivey, "Acceleration and the critical heat flux in pool boiling heat transfer," *Proc. Inst. Mech. Eng.*, vol. 177, no. 1, pp. 15–42, 1963.
- [26] M. Jakob and W. Fritz, "Versuche über den verdampfungsvorgang," *Forsch. Auf Dem Geb. Ingenieurwesen*, vol. 2, pp. 435–447, 1931.
- [27] E. Teodori, A. S. Moita, and A. L. N. Moreira, "Empirical Correlations Between Bubble Dynamics and Heat Transfer Coefficient for Pool Boiling Over Micro-Textured Surfaces," p. 15, 2014.

APPENDIX - I:

SPECIFICATION OF EQUIPMENT

1. Copper Block

Thermal Expansion Coefficient :	16.5 $\mu\text{m}/(\text{m}\cdot\text{K})$ (at 25 °C)
Thermal Conductivity :	401 $\text{W}/(\text{m}\cdot\text{K})$
Density :	8940 kg/m^3
Specific Heat :	385 $\text{J}/\text{kg}\cdot\text{°C}$
Thermal Diffusivity :	1.11×10^{-4} m^2/s (at 25 °C)
Melting Point :	1,085 °C

2. Camera

Brand :	Phantom
Model :	MIRO EX4096MC
Sensor :	CMOS
Color Depth :	8/12 bit
FPS :	500-1260 FPS at full resolution (800x600) 111,100fps at lowest resolution (32x16 pixel)
ISO :	4800 (Monochrome) & 1200 (Color)

3. Heater

Maximum Voltage :	220 Volts
Maximum Current :	5 A
Power :	1000 W

4. Working Fluid

Type :	Water
Chemical formula :	H_2O

Molar mass	:	18.01528(33) g/mol
Density	:	0.9998396 g/mL at 0 °C 0.9970474 g/mL at 25 °C 0.961893 g/mL at 95 °C 0.9167 g/ml at 0 °C (Solid)
Melting point	:	0.00 °C (32.00 °F; 273.15 K)
Boiling point	:	99.98 °C (211.96 °F; 373.13 K)
Vapor pressure	:	3.1690 kilo-pascals or 0.031276 atm
Thermal conductivity	:	0.6065 W/(m·K)
Refractive index (n _D)	:	1.3330 (20 °C)
Viscosity	:	0.890 cP

APPENDIX - II: DATA TABLES

Surface Type = Plain

ΔT = Wall superheat (K)
 q = Corrected heat flux (kW/m²)
 h_f = Heat transfer coefficient (kW/m²K)
 d_b = Bubble departure diameter (mm)
 f_d = Bubble departure frequency (Hz)

Table. A: Collected data during experiment, plain surface

Observation No.	ΔT , (K)	q , (kW/m ²)	h_f , (kW/m ² K)	d_b , (mm)	f_d , (Hz)
1	2	3.00	1.50	1.80	5
2	4	8.00	2.00	1.85	8
3	6	13.00	2.17	1.90	14
4	8	18.00	2.25	2.24	19
5	10	24.00	2.40	2.32	23
6	12	31.00	2.58	2.41	28
7	14	41.00	2.93	2.73	31
8	16	55.00	3.44	3.11	46
9	18	71.00	3.94	3.24	58
10	20	81.00	4.05	3.32	59
11	22	92.00	4.18	3.38	71
12	24	101.00	4.21	3.41	83
13	26	113.00	4.35	3.50	97
14	28	125.00	4.46	3.60	101

Surface Type = Pitted

ΔT = Wall superheat (K)
 q = Corrected heat flux (kW/m²)
 h_f = Heat transfer coefficient (kW/m²K)
 d_b = Bubble departure diameter (mm)
 f_d = Bubble departure frequency (Hz)

Table. B: Collected data during experiment, Pitted surface, 20 pits

Observation No.	ΔT , (K)	q , (kW/m ²)	h_f , (kW/m ² K)	d_b , (mm)	f_d , (Hz)
1	2	5.00	2.50	1.90	21
2	4	14.00	3.50	1.90	28
3	6	22.00	3.67	2.20	29
4	8	38.00	4.75	2.40	27
5	10	51.00	5.10	2.60	45
6	12	70.00	5.83	2.80	78
7	14	91.00	6.50	3.20	92
8	16	110.00	6.88	3.30	101
9	18	124.00	6.89	3.60	97
10	20	140.00	7.00	3.80	122
11	22	161.00	7.32	3.80	130
12	24	181.00	7.54	4.00	153
13	26	200.00	7.69	4.00	173
14	28	220.00	7.86	4.10	190

Table. C: Collected data during experiment, Pitted surface, 25 pits

Observation No.	ΔT , (K)	q , (kW/m ²)	h_f , (kW/m ² K)	d_b , (mm)	f_d , (Hz)
1	2	5.50	2.75	2.00	21
2	4	14.10	3.53	2.00	27
3	6	23.00	3.83	2.20	29
4	8	39.10	4.89	2.40	31
5	10	53.40	5.34	2.70	43
6	12	72.00	6.00	3.20	45
7	14	91.10	6.51	3.50	89
8	16	110.00	6.88	3.50	110
9	18	124.00	6.89	3.70	113
10	20	143.00	7.15	3.90	139
11	22	166.00	7.55	4.00	154
12	24	181.00	7.54	4.20	167
13	26	203.00	7.81	4.20	189
14	28	220.00	7.86	4.30	191

Table. D: Collected data during experiment, Pitted surface, 35 pits

Observation No.	ΔT , (K)	q , (kW/m ²)	h_f , (kW/m ² K)	d_b , (mm)	f_d , (Hz)
1	2	5.50	2.75	2.10	23
2	4	15.00	3.75	2.10	31
3	6	23.50	3.92	2.40	33
4	8	39.50	4.94	2.50	30
5	10	55.00	5.50	2.80	48
6	12	75.00	6.25	3.30	91
7	14	91.00	6.50	3.60	110
8	16	111.00	6.94	3.70	110
9	18	125.00	6.94	3.80	119
10	20	143.00	7.15	4.00	115
11	22	169.00	7.68	4.10	131
12	24	192.00	8.00	4.10	168
13	26	209.00	8.04	4.20	175
14	28	229.00	8.18	4.30	188

Surface Type = Finned

- ΔT = Wall superheat (K)
 q = Corrected heat flux (kW/m²)
 h_f = Heat transfer coefficient (kW/m²K)
 d_b = Bubble departure diameter (mm)
 f_d = Bubble departure frequency (Hz)

Table. E: Collected data during experiment, Finned surface

Observation No.	ΔT , (K)	q , (kW/m ²)	h_f , (kW/m ² K)	d_b , (mm)	f_d , (Hz)
1	2	8.00	4.00	2.20	57
2	4	17.60	4.40	2.30	79
3	6	31.00	5.17	2.50	94
4	8	51.00	6.38	2.50	103
5	10	72.00	7.20	2.90	109
6	12	89.00	7.42	3.10	101
7	14	105.00	7.50	3.30	119
8	16	135.00	8.44	3.60	148
9	18	155.00	8.61	3.60	193
10	20	177.00	8.85	3.70	234
11	22	198.00	9.00	3.90	263
12	24	240.00	10.00	4.10	289
13	26	280.00	10.77	4.30	291

APPENDIX - III: SAMPLE CALCULATION

1. Plain Surface:

For observation no. 2:

Radius of the surface = 24.5mm or 0.0245m

Area of the surface, $A = \pi r^2 = \pi \times (.0245)^2 = 1.89 \times 10^{-3} \text{ m}^2$

Electric power supplied, $P = VI \cos \theta$

For observation no 2,

Voltage, $V = 60$ volts

Current supply, $I = 0.3$ ampere

So, total electric power supplied, $P = (60 \times 0.3 \times 0.85)$ watts = 15.3 watts

Heat flux, $q_s = \frac{15.3}{1.89 \times 10^{-3}} \text{ W/m}^2 = 8095.23 \text{ W/m}^2$

Heat loss $q_L = 161.6 \text{ W/m}^2$

Total heat flux, $q = q_s - q_L = (8095.23 - 161.6) \text{ W/m}^2 = 7933 \text{ W/m}^2 = 8 \text{ kW/m}^2$ (approx.)

2. Finned Surface:

For observation no. 2:

Radius of the surface = 24.5mm or 0.0245m

Area of the surface, $A = \pi r^2 = \pi \times (.0245)^2 = 1.89 \times 10^{-3} \text{ m}^2$

Radius of the fin, $r_f = 1.25$ mm or 0.00125m

Height of fins, $h_f = 5$ mm = 0.005m

Surface area of the fin $A_f = 2 \pi (0.00125) (0.005) = 3.9 \times 10^{-5} \text{ m}^2$

Number of fins, $N = 47$

Total surface area = $A + N \times A_f = 0.00189 + (47 \times 0.000039) = 0.003723 \text{ m}^2$

Electric power supplied, $P = VI \cos \theta$

Voltage, $V = 100$ volts

Current supply, $I = 0.8$ ampere

So, total electric power supplied, $P = (100 \times 0.8 \times 0.85)$ watts = 68 watts

$$\text{Heat flux, } q_s = \frac{68}{0.003723} \text{ W/m}^2 = 18264.84 \text{ W/m}^2$$

$$\text{Heat loss } q_L = 667 \text{ W/m}^2$$

$$\text{Total heat flux, } q = q_s - q_L = (18264.84 - 667) \text{ W/m}^2 = 17597.84 \text{ W/m}^2 = 17.6 \text{ kW/m}^2 (\text{approx})$$

3. Pitted Surface:

For observation no. 2:

Radius of the surface = 24.5mm or 0.0245m

$$\text{Area of the surface, } A = \pi r^2 = \pi \times (.0245)^2 = 1.89 \times 10^{-3} \text{ m}^2$$

Radius of the pit, $r_p = 1 \text{ mm} = 0.001 \text{ m}$

Depth of pit, $h_p = 1 \text{ mm} = 0.001 \text{ m}$

$$\text{Surface area of the pit } A_p = 2 \pi (0.001) (0.001) = 6.28 \times 10^{-6} \text{ m}^2$$

Number of pits, $N = 20$

$$\text{Total surface area} = A + N \times A_p = 0.00189 + (20 \times 0.00000628) = 0.002 \text{ m}^2$$

Electric power supplied, $P = VI \cos \theta$

Voltage, $V = 85$ volts

Current supply, $I = 0.4$ ampere

So, total electric power supplied, $P = (85 \times 0.4 \times 0.85)$ watts = 28.9 watts

$$\text{Heat flux, } q_s = \frac{28.9}{0.002} \text{ W/m}^2 = 14450 \text{ W/m}^2$$

$$\text{Heat loss } q_L = 452.5 \text{ W/m}^2$$

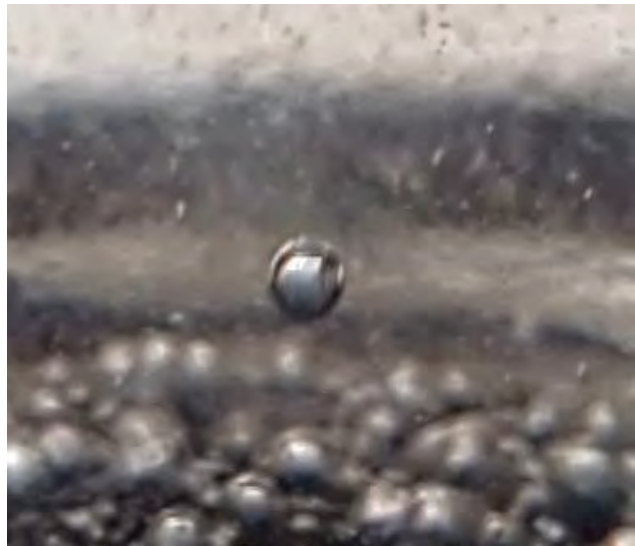
$$\text{Total heat flux, } q = q_s - q_L = (14450 - 452.5) \text{ W/m}^2 = 13997.5 \text{ W/m}^2 = 14 \text{ kW/m}^2 (\text{approx})$$

APPENDIX - IV: IMAGES

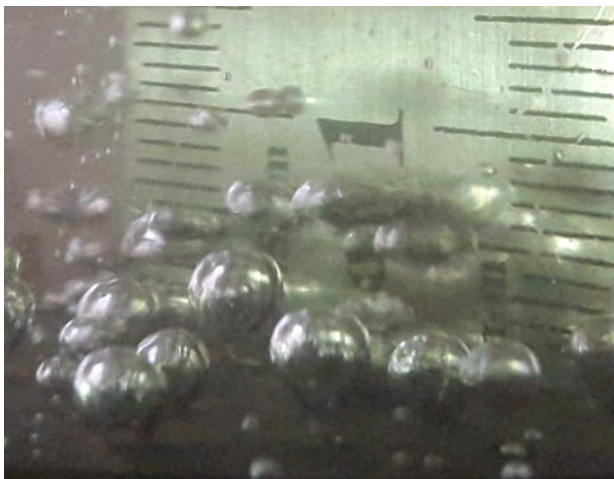
Bubble activity on the plain surface



$\Delta T = 2K; q = 3 \text{ kW/m}^2$



$\Delta T = 8K ; q = 13 \text{ kW/m}^2$



$\Delta T = 16K; q = 55 \text{ kW/m}^2$



$\Delta T = 28K ; q = 125 \text{ kW/m}^2$



$\Delta T = 20K; q = 92 \text{ kW/m}^2$



$\Delta T = 14K; q = 50 \text{ kW/m}^2$



$\Delta T = 10K; q = 25 \text{ kW/m}^2$

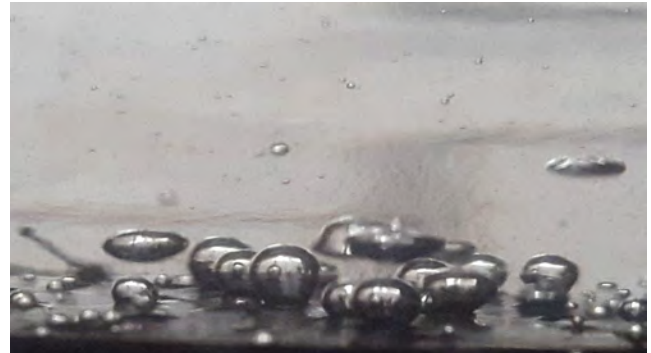


$\Delta T = 12K; q = 30 \text{ kW/m}^2$

Bubble activity on pitted surface



$\Delta T = 2K; q = 5.50 \text{ kW/m}^2$



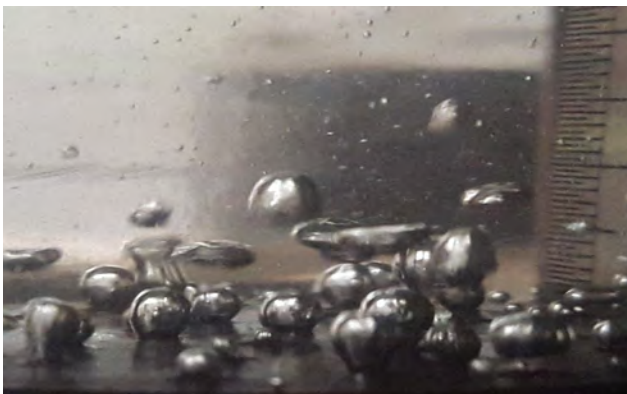
$\Delta T = 8K; q = 39.50 \text{ kW/m}^2$



$\Delta T = 18K; q = 125 \text{ kW/m}^2$



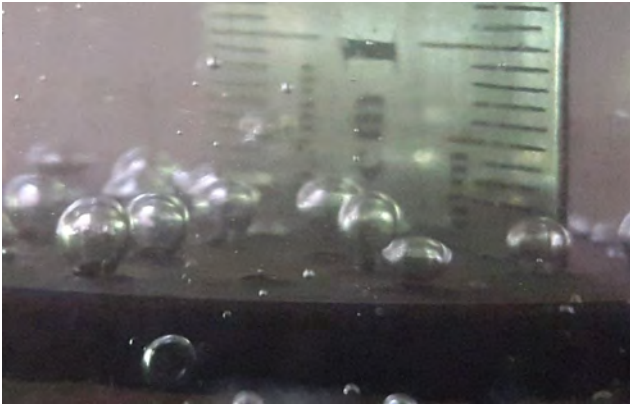
$\Delta T = 14K; q = 91 \text{ kW/m}^2$



$\Delta T = 16K; q = 111 \text{ kW/m}^2$



$\Delta T = 24K; q = 192 \text{ kW/m}^2$



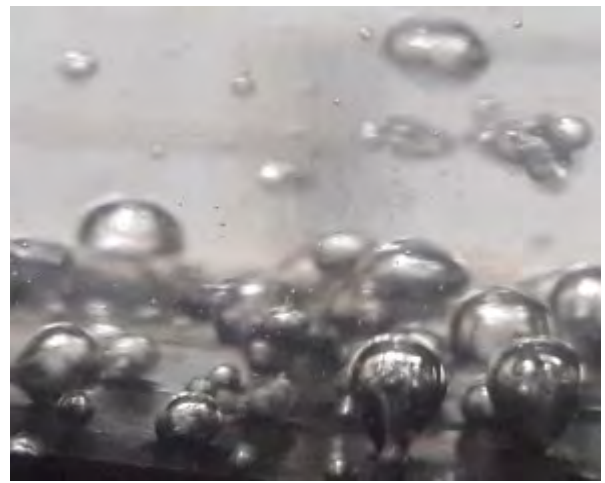
$\Delta T = 6K; q = 25 \text{ kW/m}^2$



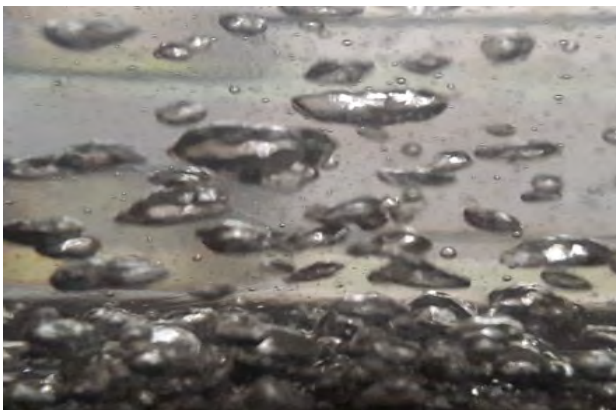
$\Delta T = 10K; q = 52 \text{ kW/m}^2$



$\Delta T = 16K; q = 102 \text{ kW/m}^2$



$\Delta T = 12K; q = 55 \text{ kW/m}^2$



$\Delta T = 20K; q = 145 \text{ kW/m}^2$

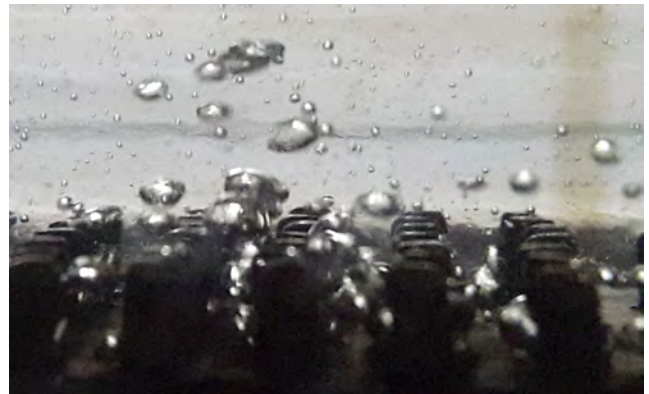


$\Delta T = 22K; q = 155 \text{ kW/m}^2$

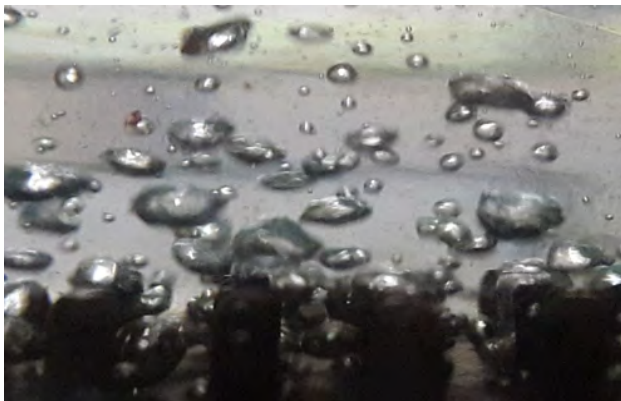
Bubble activity on finned surface



$\Delta T = 2K; q = 17.6 \text{ kW/m}^2$



$\Delta T = 8K; q = 72 \text{ kW/m}^2$



$\Delta T = 12K; q = 135 \text{ kW/m}^2$



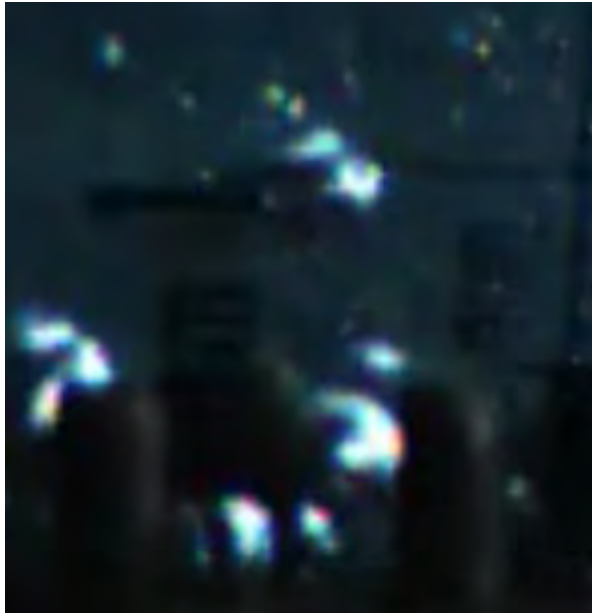
$\Delta T = 16K; q = 177 \text{ kW/m}^2$



$\Delta T = 20K; q = 240 \text{ kW/m}^2$



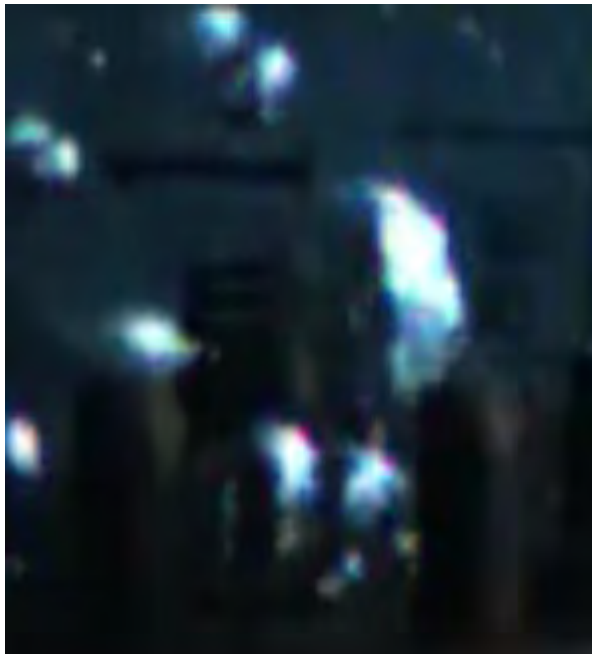
$\Delta T = 18K; q = 198 \text{ kW/m}^2$



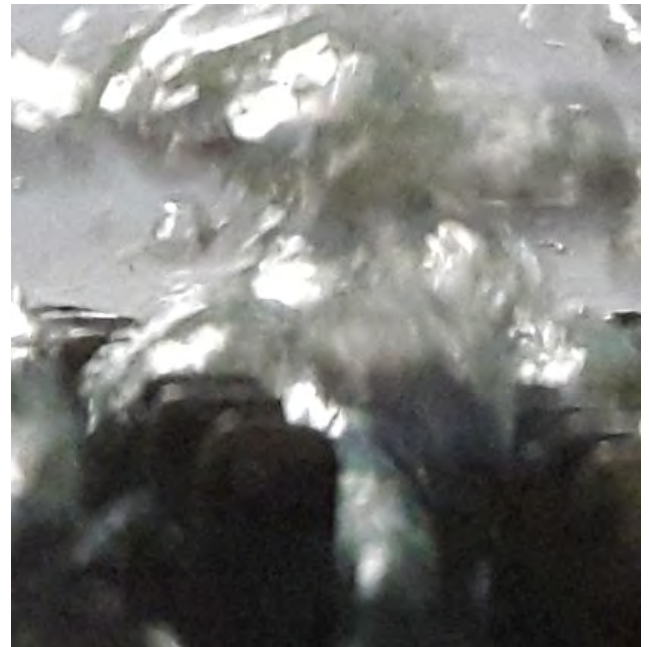
$\Delta T = 10K; q = 78 \text{ kW/m}^2$



$\Delta T = 14K; q = 112 \text{ kW/m}^2$



$\Delta T = 20K; q = 202 \text{ kW/m}^2$



$\Delta T = 24K; q = 280 \text{ kW/m}^2$

APPENDIX - V: UNCERTAINTY ANALYSIS

Experimental measurements are prone to having a certain amount of error. The error is often caused by degree of error of the used instruments and measurement techniques. It results in deviation of experimental values from actual values. Hence, the term uncertainty is introduced. It is used to refer to the possible error that a value can contain.

Two types of error can occur, one is systematic error and the other one is measuring error. The systematic error occurs usually by un-calibrated or mis-calibrated instrument. The measuring error can occur for relative mis-observation or measuring values larger or smaller than it actually is. For single measurement the uncertainty is a fixed number. But this particular value can vary considering the particular circumstances of observation.

1. Uncertainties in Measurands:

Now-a-days experimenters are advised to report the uncertainties in every measurand considering the following information:

- a. *Precision limit, P* : This is an estimate of the lack of repeatability caused by random errors and process unsteadiness. This element can be sampled with the available procedure and apparatus, and should be based on statistical estimates from samples whenever possible.
- b. *Bias limit, B* : The bias limit is an estimate of the magnitude of the fixed constant error. This element can not be sampled within available procedure and its existence is what mandates the need of cross-checks.
- c. *Uncertainty, W*: The ± 5 interval about the nominal results is the band within which the experiment is 95% confident that the true value of the result lies. And it is calculated from the following:

$$W=[P^2 + B^2]^{1/2}$$

2. Propagation of Uncertainties Into Results:

In calibration experiments, one measures the desired result directly. No problem of uncertainty then arises; we have desired results in hand once we complete measurements. In nearly all other

experiments, it is necessary to compute the uncertainty in the results from the estimates of uncertainty in the measurands. This computation process is called “propagation of uncertainty”.

According to Kline and McClintock (1953), the propagation equation of a result R computed from n measurands $x_1, x_2, x_3, \dots, x_n$ having absolute uncertainty W_R is given by the following equation:

$$W_R = \left[\left(\frac{\partial R}{\partial x_1} w_{x1} \right)^2 + \left(\frac{\partial R}{\partial x_2} w_{x2} \right)^2 + \dots + \left(\frac{\partial R}{\partial x_n} w_{xn} \right)^2 \right]^{1/2}$$

Which can be considered separately in computing the precision and bias components of uncertainties when the function of R is known

3. Uncertainties in the Present Experiment

The uncertainty of particular instruments used in the experiment is listed below:

Instrument	Uncertainty
Digital Thermometer with K-Thermocouple	±0.1 K
Voltage Controller (Variac)	±1V
Multi-meter (Current)	±0.1A

The uncertainty of measurement carried out during the experiment is listed below:

Parameter	Uncertainty
Surface Temperature (K)	±1.16%
Heat flux, q(W/m ²)	±1.2%
Power (W)	±1.3%
Bubble Diameter (mm)	±6%
Bubble frequency (Hz)	±12%